



Developing Enhanced Curve Advisory Speed and Curve Safety Assessment Guidelines

Technical Report 0-6960-R1

Cooperative Research Program

TEXAS A&M TRANSPORTATION INSTITUTE
COLLEGE STATION, TEXAS

in cooperation with the
Federal Highway Administration and the
Texas Department of Transportation
<http://tti.tamu.edu/documents/0-6960-R1.pdf>

1. Report No. FHWA/TX-19/0-6960-R1		2. Government Accession No.		3. Recipient's Catalog No.	
4. Title and Subtitle DEVELOPING ENHANCED CURVE ADVISORY SPEED AND CURVE SAFETY ASSESSMENT GUIDELINES				5. Report Date Published: May 2019	
				6. Performing Organization Code	
7. Author(s) Michael P. Pratt, Srinivas R. Geedipally, Raul E. Avelar, Minh Le, and Dominique Lord				8. Performing Organization Report No. Report 0-6960-R1	
9. Performing Organization Name and Address Texas A&M Transportation Institute The Texas A&M University System College Station, Texas 77843-3135				10. Work Unit No. (TRAIS)	
				11. Contract or Grant No. Project 0-6960	
12. Sponsoring Agency Name and Address Texas Department of Transportation Research and Technology Implementation Office 125 E. 11th Street Austin, Texas 78701-2483				13. Type of Report and Period Covered Technical Report: September 2017–February 2019	
				14. Sponsoring Agency Code	
15. Supplementary Notes Project performed in cooperation with the Texas Department of Transportation and the Federal Highway Administration. Project Title: Enhancing Curve Advisory Speed and Curve Safety Assessment Practices URL: http://tti.tamu.edu/documents/0-6960-R1.pdf					
16. Abstract The Texas Department of Transportation (TxDOT) is in the process of conducting several parallel efforts to evaluate rural highway horizontal curves. Following the adoption of the 2011 <i>Texas Manual on Uniform Traffic Control Devices</i> , district personnel are checking and updating posted curve advisory speeds and other curve traffic control devices (e.g., Chevrons) in response to the December 31, 2019, compliance date. Recent legislation has allowed regulatory speed limits to be increased to 75 mph on some rural highways, resulting in a need to check and evaluate curves that had not previously been signed with advisory speeds. There is also renewed interest in implementing pavement friction treatments through the Highway Safety Improvement Program. In this research project, researchers collected and analyzed data to extend TxDOT's curve advisory speed setting procedures to rural multilane highways and freeways as well as two-lane rural highways with speed limits of 75 mph. Researchers also improved TxDOT's global positioning system (GPS)-based curve measurement system's capabilities to measure grade. Finally, the researchers drafted the <i>Horizontal Curve Evaluation Handbook</i> to aid TxDOT's practitioners in using the GPS-based system for evaluating curves.					
17. Key Words Traffic Control Devices, Warning Signs, Speed Signs, Speed Measurement, Trucks, Traffic Speed, Highway Safety, Rural Highways, Highway Curves, Crash, Crash Risk			18. Distribution Statement No restrictions. This document is available to the public through NTIS: National Technical Information Service Alexandria, Virginia 22312 http://www.ntis.gov		
19. Security Classif. (of this report) Unclassified		20. Security Classif. (of this page) Unclassified		21. No. of Pages 60	22. Price

DEVELOPING ENHANCED CURVE ADVISORY SPEED AND CURVE SAFETY ASSESSMENT GUIDELINES

by

Michael P. Pratt, P.E.
Assistant Research Engineer
Texas A&M Transportation Institute

Srinivas R. Geedipally, Ph.D., P.E.
Associate Research Engineer
Texas A&M Transportation Institute

Raul E. Avelar, Ph.D., P.E.
Associate Research Engineer
Texas A&M Transportation Institute

Minh Le, P.E.
Associate Research Engineer
Texas A&M Transportation Institute

and

Dominique Lord, Ph.D.
Professor
Texas A&M University

Report 0-6960-R1
Project 0-6960

Project Title: Enhancing Curve Advisory Speed and Curve Safety Assessment Practices

Performed in cooperation with the
Texas Department of Transportation
and the
Federal Highway Administration

Published: May 2019

TEXAS A&M TRANSPORTATION INSTITUTE
College Station, Texas 77843-3135

DISCLAIMER

This research was performed in cooperation with the Texas Department of Transportation (TxDOT) and the Federal Highway Administration (FHWA). The contents of this report reflect the views of the authors, who are responsible for the facts and the accuracy of the data published herein. The contents do not necessarily reflect the official view or policies of FHWA or TxDOT. This report does not constitute a standard, specification, or regulation. It is not intended for construction, bidding, or permitting purposes. The engineer in charge of the project was Michael P. Pratt, P.E. #102332.

The United States Government and the State of Texas do not endorse products or manufacturers. Trade or manufacturers' names appear herein solely because they are considered essential to the object of this report.

ACKNOWLEDGMENTS

TxDOT and FHWA sponsored this research project. Mr. Michael Pratt, Dr. Srinivas Geedipally, Dr. Raul Avelar, and Mr. Minh Le with the Texas A&M Transportation Institute, and Dr. Dominique Lord with Texas A&M University prepared this report.

The researchers acknowledge the support and guidance that the Project Monitoring Committee provided:

- Mr. Darrin Jensen, Project Manager (TxDOT, Research and Technology Implementation Office).
- Ms. America Garza (TxDOT, Corpus Christi District).
- Ms. Kassondra Muñoz (TxDOT, Corpus Christi District).
- Mr. Jeff Miles (TxDOT, Bryan District).
- Mr. Maurice Maness (TxDOT, Bryan District).
- Mr. Jacob Chau (TxDOT, Waco District).
- Mr. Bahman Afsheen (TxDOT, Dallas District).
- Mr. Donald Maddux (TxDOT, Lufkin District).
- Ms. Patti Dathe, Contract Specialist (TxDOT, Research and Technology Implementation Office).

In addition, researchers acknowledge the valuable contributions of Mr. Hassan Charara, Mr. Dan Walker, Mr. Kyle Kingsbury, Ms. Diana Wallace, Mr. Gary Barricklow, Ms. Christa Winburn, Ms. Katherine Lufkin, Mr. Marc Garcia, and Mr. Eder Fuabuna Suenge, who assisted with various tasks during the conduct of the project.

TABLE OF CONTENTS

List of Figures	viii
List of Tables	ix
Chapter 1: Overview	1
Introduction.....	1
Research Approach	1
Chapter 2: Literature Review	3
Introduction.....	3
Vehicle Speeds on Curves	3
Curve Safety Trends	10
Data Signal and Noise Processing Trends	12
Chapter 3: Curve Speed Data Collection and Analysis	17
Introduction.....	17
Speed Data Collection Plan	17
Database Attributes.....	17
Data Collection Methods	18
Site Selection and Screening.....	19
Data Summary	19
Data Collection Site Characteristics	20
Speed Data Preliminary Analysis	22
Model Calibration	26
Two-Lane Undivided Highways with 75-mph Regulatory Speed Limits	26
Four-Lane Highways	30
Other Empirical Relationships.....	33
Chapter 4: Software Development and Analysis of Elevation Data	35
Introduction.....	35
Software Program Description and Updates.....	35
Roadway Elevation Data Analysis and Grade Calculation.....	38
Preliminary Analysis.....	39
Modeling Grade as a Function of Device Data.....	40
Codependency Error Structure.....	43
References	47

LIST OF FIGURES

Figure 1. Average Truck Speed as a Function of Radius and Approach Speed.	5
Figure 2. Curve Radius Crash Modification Factor.....	11
Figure 3. Raw and Kalman-Filtered Heading Change Data.	13
Figure 4. Aggregated Filtered Heading Change Data with Sixth-Order Polynomial.	13
Figure 5. Example of Smoothing Curve on a Noisy Speed Signal.	15
Figure 6. Speed Data Collection Site Locations.	21
Figure 7. Comparison of Measured and Predicted Approach Tangent Speeds for Two-Lane Highways.	27
Figure 8. Comparison of Measured and Predicted Curve Speeds for Two-Lane Highways.....	30
Figure 9. Comparison of Measured and Predicted Curve Speeds for Four-Lane Highways.....	31
Figure 10. Comparison of Measured and Predicted Curve Speeds for Four-Lane Highways.....	33
Figure 11. TRAMS upon Startup.....	37
Figure 12. TRAMS in Use.....	37
Figure 13. Raw and Smoothed Ball-Bank Indicator Readings.	38
Figure 14. TCES List Worksheet.....	38
Figure 15. Comparison of Barometric and GPS Elevation.....	39
Figure 16. Adjusted Comparison of Barometric and GPS Elevation.	40
Figure 17. Comparison of Measured and Ground-Truth Grade.	41
Figure 18. Comparison of Three Grade Measurement Time Series at Blue Ridge Site.....	42
Figure 19. Performance of Grade-Calculation Model at Koppe Bridge Site.....	45
Figure 20. Comparison of Estimated and Actual Grade.	46

LIST OF TABLES

Table 1. Curve Speed Models for Rural Two-Lane Highways.	5
Table 2. Curve Speed Models for Rural Multilane Highways.....	8
Table 3. Curve Delineation CMFs.	12
Table 4. Site Description Data.	18
Table 5. Site Location and Traffic Control Characteristics.	20
Table 6. Site Geometric Characteristics.....	22
Table 7. Site Pavement Characteristics.....	23
Table 8. Vehicle Counts by Site.	24
Table 9. Matched Free-Flow Vehicles by Site.....	25
Table 10. Model Calibration Matrix.	26
Table 11. Approach Tangent Speed Model Calibration Results for Two-Lane Highways.	27
Table 12. Two-Lane Highway Approach Tangent Speed Model Predictions.	28
Table 13. 85 th Percentile Curve Speed Model Calibration Results for Two-Lane Highways.	28
Table 14. Average Curve Speed Model Calibration Results for Two-Lane Highways.....	29
Table 15. Two-Lane Highway Curve Speed Model Predictions.	30
Table 16. Approach Tangent Speed Model Calibration Results for Four-Lane Highways – Right Lane	31
Table 17. Curve Speed Model Calibration Results for Four-Lane Highways.....	32
Table 18. Truck Speed as a Function of Passenger Car Speed at Approach Tangents.....	33
Table 19. Average Passenger Car Speed as a Function of 85 th -Percentile Passenger Car Speed at Approach Tangents.	34
Table 20. Average Left-Lane Passenger Car Speed as a Function of Average Right-Lane Passenger Car Speed at Approach Tangents.	34
Table 21. Grade Time Series Model Calibration Results.	45

CHAPTER 1: OVERVIEW

INTRODUCTION

Horizontal curves are a necessary part of the highway system, but statistics have consistently shown that curves represent significant safety concerns. These concerns arise from the increased driver workload associated with traversing a curve, driver errors like failing to detect a curve or judge its sharpness correctly, and the possibility of obtaining inadequate side friction supply from the tire-pavement interface in inclement weather conditions.

The provision of a properly determined advisory speed is an important part of warning drivers about the severity of an upcoming curve. The advisory speed also forms the basis for choosing other curve traffic control devices, like Chevrons, based on the guidance provided in the *Texas Manual on Uniform Traffic Control Devices* (TMUTCD) (1). Based on previous research and implementation projects, the Texas Department of Transportation (TxDOT) successfully updated the guidelines for setting curve advisory speeds on rural two-lane highway curves. Additional research was needed to extend this guidance to rural multilane highways and freeways, as well as to validate the guidance for two-lane highways that have higher speed limits (≥ 75 mph) than what existed when the current guidance was developed.

RESEARCH APPROACH

The research team collected new speed data on curves and their approach tangents on the rural highway types of interest. These highways included two-lane highways with regulatory speed limits of 75 mph, four-lane undivided highways, four-lane divided highways, and four-lane freeways. The assembled database included approximately 39,000 vehicles observed in daytime free-flow conditions across 38 curve sites. The research team then calibrated curve speed prediction models to be used in setting curve advisory speeds. The models were based on previously developed models for two-lane highways with speed limits of 70 mph or lower (2).

The research team collected elevation data on several rural highway curve sites using a global positioning system (GPS) receiver and a barometer and examined methods to compute grade from the elevation measurements. By comparing the collected data with ground-truth grade measurements, the research team developed a model to estimate roadway grade using GPS-measured elevation.

The research team updated the Texas Roadway Analysis and Measurement Software (TRAMS) program that was previously developed in TxDOT Implementation Project 5-5439 (3) and developed a new Excel[®]-based spreadsheet program called Texas Curve Evaluation Suite (TCES) to accompany the updated TRAMS program. These resources are designed to work with a GPS receiver and an electronic ball-bank indicator to collect the required data to implement TxDOT's GPS Method for setting curve advisory speeds (4) and to facilitate an analysis of curve pavement skid resistance (5, 6).

CHAPTER 2: LITERATURE REVIEW

INTRODUCTION

The provision of a properly determined advisory speed is an important part of warning drivers about the severity of an upcoming curve. The advisory speed also forms the basis for choosing other curve traffic control devices, like Chevrons, based on the guidance provided in the TMUTCD (1). Based on previous research and implementation projects, TxDOT successfully updated the guidelines for setting curve advisory speeds on rural two-lane highway curves. Research is now needed to extend this guidance to rural multilane highways and freeways, as well as to validate the guidance for two-lane highways that have higher speed limits (≥ 75 mph) than what existed when the current guidance was developed.

Statistics have consistently shown that the crash rate on horizontal curves is significantly greater than that on tangent roadway segments of similar character. This trend may be caused by drivers failing to detect the presence of a curve or attempting to negotiate the curve at unsafe speeds. In TxDOT Research Project 0-6031, Lord et al. examined the effects of roadway geometry, curve presence and density, weather, and other factors on roadway departure crashes in Texas (7). Their findings confirmed the general trends that crash rates on rural highways are influenced by both presence and sharpness of horizontal curvature, and that curve-related crashes are more frequent on higher-speed roadways. They found that the fatal-and-injury roadway departure crash rate in Texas is 1.9 per million vehicle miles for tangent highway segments and 4.2 per million vehicle miles for curved highway segments.

This chapter consists of three parts. The first part summarizes past research on vehicle speeds on highway curves. The second part provides perspectives on curve safety trends. The third part discusses data signal and noise processing methods.

VEHICLE SPEEDS ON CURVES

The American Association of State Highway and Transportation Official's (AASHTO's) *A Policy on Geometric Design of Highways and Streets (Green Book)* states that the design of horizontal curves should be based on a proper relationship between speed, curvature, superelevation rate, and side friction demand (8). The *Green Book* offers the following equation to describe the relationship between these variables:

$$f_D = \frac{v^2}{gR} - \frac{e}{100} \quad (1)$$

where:

- f_D = side friction demand (lateral acceleration divided by g);
- v_c = curve speed, ft/s;
- g = gravitational constant (= 32.2 ft/s²);
- R = curve radius, ft; and
- e = superelevation rate, percent.

This equation is referred to as the point-mass model. It shows that the side friction demand of a vehicle traveling at a given speed increases as curve radius or superelevation rate decrease. For design purposes, the *Green Book* recommends side friction factors that represent driver comfort limits. These factors are used to determine an appropriate curve radius and superelevation rate for the roadway's design speed.

In their efforts to develop guidelines for determining advisory speeds on rural two-lane highways, Bonneson et al. theorized the following functional form for the relationship between vehicle speeds and side friction demand (2):

$$f_D = b_0 - b_1 v_T + b_2 (v_T^2 - v_c^2) I_v \quad (2)$$

where:

- v_t = approach tangent speed;
- b_i = calibration coefficients; and
- I_v = indicator variable (= 1.0 if $v_t > v_c$, 0.0 otherwise).

By setting Equations 1 and 2 equal and solving for v_c , Bonneson et al. derived a curve speed model, which they then calibrated using a dataset of 6677 passenger cars and 1741 trucks at 41 curve sites in Texas. The resulting model for average vehicle speed on a curve is described as follows:

$$v_{c,50} = \sqrt{\frac{15.0R_p \left(0.112 - 0.00066v_{t,50} + 0.000091v_{t,50}^2 - 0.108I_{tk} + \frac{e}{100} \right)}{1 + 0.00136R_p}} \leq v_{t,50} \quad (3)$$

with:

$$R_p = R + \frac{3.0}{1 - \cos \frac{\Delta}{2}} \quad (4)$$

where:

- $v_{c,50}$ = average curve speed, mph;
- $v_{t,50}$ = average approach tangent speed, mph;
- R_p = travel path radius, ft;
- Δ = curve deflection angle, degrees; and
- I_{tk} = indicator variable for trucks (= 1.0 if predicting truck speed, 0.0 otherwise).

Equation 4 forms the basis for TxDOT's curve advisory speed guidelines, which call for the advisory speed to be set based on the average truck speed (4). Equation 4 is shown graphically in Figure 1. To apply the guidelines, the analyst must collect the required data (radius, deflection angle, superelevation rate, and approach tangent speed) to describe the curve. In TxDOT Implementation Project 5-5439, Bonneson et al. developed the GPS Method as an engineering study method to facilitate field measurement of these key variables (3). The GPS Method involves driving through the curve of interest with a GPS receiver, an electronic ball-

bank indicator, and a laptop computer, using the TRAMS program and the Texas Curve Advisory Speed (TCAS) spreadsheet to process the data. The TRAMS and TCAS programs provide curve geometric information, the recommended curve advisory speed, and the recommended or required curve traffic control devices.

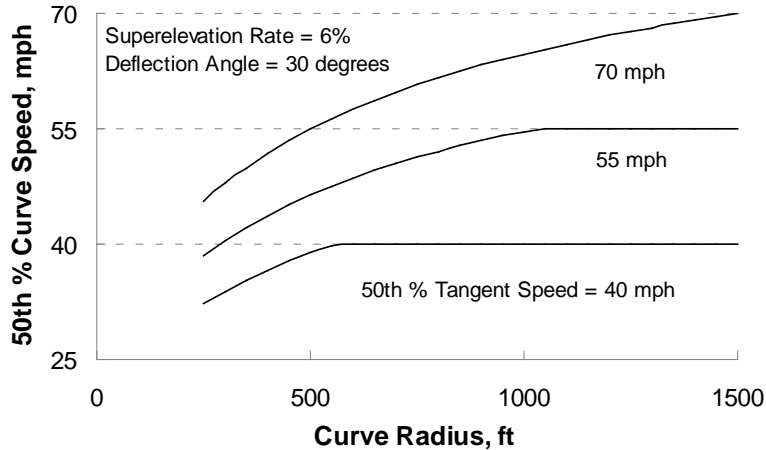


Figure 1. Average Truck Speed as a Function of Radius and Approach Speed.

Table 1 provides a list of curve speed models for rural two-lane highways. All of the models were calibrated using spot speed data, most included variables to account for curve radius (either directly or in terms of degree of curve), and some included variables to account for approach tangent speed or desired speed. The models are described in the following paragraphs.

Table 1. Curve Speed Models for Rural Two-Lane Highways.

Author(s)	Significant Variables*	Data Measures	Measurement Tools
Bonneson et al. (2)	R, V_t , Δ , e	Spot speeds	Roadway sensors
McLean, J. (9)	$1/R$, V_f	Spot speeds	Not specified
Kanellaidis et al. (10)	$1/R$, V_f	Spot speeds	Not specified
Lamm et al. (11)	DC, LW, SW, AADT	Spot speeds	Measured time over distance
Cruzado et al. (12)	Terrain type, vertical alignment, R, LW	Spot speeds	Data equipment
Ottesen and Krammes (13)	R, L_c , $L_c \times \Delta$, V_t	Spot speeds	Radar guns
Collins and Krammes (14)	$1/R$, L_c , $L_c \times \Delta$	Spot speeds	Infrared photoelectric sensors
Misaghi and Hassan (15)	R	Spot speeds	Radar guns
Schurr et al. (16)	Δ , L_c , grade	Spot speeds	Detector

* AADT = annual average daily traffic, L_c = length of curve, R = curve radius, e = superelevation rate, Δ = deflection angle, L_t = length of tangent, V_f = desired speed of 85th-percentile passenger car, DC = degree of curve, LW = lane width, SW = shoulder width, V_t = 85th-percentile approach tangent speed.

Recent research, particularly overseas, has shown that the speed at which motorists wish to drive on a particular section of highway, or the desired speed, is a good estimator of the operating speeds along a curve (9, 10). The desired speed is the speed at which drivers choose to travel under free-flow conditions on good pavement when they are not constrained by alignment features such as curves, topography, or weather. Typically, these are the free-flow speeds on the

tangent sections. The speed models developed suggest that operating speed on a curve is significantly related to the curvature ($1/R$) and the desired speed (V_f).

Lamm et al. (11) analyzed 24 curve sections in New York State and concluded that wet pavement does not have an appreciable effect on operating speeds because drivers do not adjust their speeds to compensate for it. Statistical analysis showed that the relationship between operating speed and degree of curvature developed for dry pavements is also true for wet pavements as long as visibility is not affected appreciably by heavy rain (e.g., falling from a sprinkle to moderately heavy rain). Other parameters such as curve length, superelevation rate, and gradient helped the regression model, but the equation performed well without them. Minimum sight distances of 450–550 ft were provided (representing stopping sight distance of 55-mph design speed) based on another research project that observed that drivers reduce their speeds due to limited sight distance and not as much due to the danger created by lower skid resistance on wet pavements.

Cruzado et al. (12) investigated the effects of different combinations of horizontal and vertical curves on operating speeds. They collected data on 10 two-lane rural highway segments with several combinations of vertical alignment and horizontal curves in Puerto Rico. They collected free-flow speed data at five points along each horizontal curve. They observed the following for speeds along horizontal curves:

- Level and mountainous terrains showed lower horizontal curve speeds (and different patterns) when compared to rolling terrain.
- Variations existed in the speed patterns when considering horizontal curve radii. For example, the lowest speeds did not occur in the middle of the curve in some cases.
- Different patterns appeared depending on vertical alignment (level, downgrade, upgrade, crest, etc.). For example, speeds increased until the middle of the curve, then decelerated, and then accelerated again.

Speed data were modeled by applying a decision tree classification model. The model showed that driver behavior (i.e., operating speeds) was significantly influenced by terrain type, vertical alignment, radius of horizontal curve, and lane width.

Ottesen and Krammes (13) expanded on the work of Collins and Krammes (14) and developed a speed-profile model for estimating reductions in the 85th-percentile speed from approach tangents to horizontal curves on rural two-lane highways in the United States. The model is proposed as an evaluation tool to check for design consistency violations on alignments with design speeds less than 62.1 mph. The model was calibrated by using speed and geometry data collected for 138 horizontal curves and 78 approach tangents (800-ft minimum) on 29 rural highways in five states. The 85th-percentile speed on horizontal curves was best estimated by the degree of curvature followed by the length of curvature and deflection angle (i.e., statistically significant). The 85th-percentile speeds on the inside and outside lanes are not significantly different at most curves. Finally, the 85th-percentile speeds on curves with degrees of curvature less than 4 do not differ significantly from 85th-percentile speeds on long tangents.

Misaghi and Hassan (15) collected and analyzed speed data on 20 curves on two-lane rural highways in Ontario using traffic classifiers at three different points along the curves. Sites were limited to rural areas (AADT less than 10,000 veh/d), marked and paved roadways with constant lane width, no stop-controlled/signalized intersections within 0.8 km of the curve, no abnormal hazard such as a narrow bridge, and radius greater than about 3900 ft and total curve length greater than about 330 ft. They found that the speed behavior of passenger cars and light trucks differed significantly from heavy trucks. The relationship between operating speed and curve radius or other alignment parameters was relatively weak. It was also found that simple subtraction of operating speeds at the approach tangent and the middle of the curve underestimated the speed differential. Finally, the relationship between the speed differential and the geometric features was stronger than relationships between operating speed and geometric features.

Schurr et al. (16) collected and analyzed data at 40 horizontal curve sites on rural two-lane highways in Nebraska. The study focused on highways with posted speeds of 55, 60, and 65 mph in order to determine the relationship among the design, operating, and posted speeds so that guidelines for consistent roadway design along horizontal alignments could be provided. The mean, 85th-percentile, and 95th-percentile speeds were measured and analyzed only for free-flow passenger cars traveling on dry pavement during daylight hours at tangent approach and curve midpoint locations. Regression analysis found that at the midpoint location, the deflection angle increased as the mean, 85th-percentile, and 95th-percentile speed decreased. The researchers concluded that drivers may perceive large change in direction as a motivation to slow their speed. Additionally, as the curve length increased, the mean, the 85th-percentile, and the 95th-percentile speed increased. Motorists were motivated to increase their speed on longer curves, which suggests they may be more comfortable traveling at higher speeds along a longer curve because they have more time to adjust their trajectory to a constant radius. It was found that as the posted regulatory speed limit increased, so did the mean speed. Also, as the approach grade increased, the 85th-percentile speed decreased, which indicates that grade has an influence on the upper percentage range of vehicle speeds, likely because of vehicle engine performance. Finally, as the AADT increased, the 95th-percentile speed decreased. At the approach locations, the 85th-percentile and 95th-percentile speeds were influenced by posted speed and AADT. Overall, the majority of drivers tended not to reduce their speed significantly when traveling from a tangent segment to a horizontal curve (for curves with radii greater than 1146 ft).

The literature contains many models for estimating vehicle speeds on rural two-lane highway curves. However, relatively few models have been documented for multilane highways. Table 2 provides a list of models for several types of rural multilane highways.

Gong and Stamatiadis published models for the inside and outside lanes of a multilane highway curve, which are shown in Equations 5 and 6, respectively (17). Their models include terms for shoulder type, median type, pavement type, grade, curve radius, and curve length.

$$v_{c,85,i} = 51.52 + 1.567I_{ST} - 2.795I_{MT} - 4.001I_{PT} - 2.15I_{AG} + 2.221 \ln L_c \quad (5)$$

$$v_{c,85,o} = 59.26 + 1.804I_{ST} - 2.521I_{MT} - 1.071I_{AG} + 0.00047R + 2.408 \frac{L_c}{R} \quad (6)$$

where:

- $v_{c,85,i}$ = 85th-percentile speed in the inside lane of the curve, mph;
- $v_{c,85,o}$ = 85th-percentile speed in the outside lane of the curve, mph;
- I_{ST} = indicator variable for shoulder type (= 1.0 if surfaced, 0.0 otherwise);
- I_{MT} = indicator variable for median barrier type (= 1.0 if no positive barrier present, 0.0 otherwise);
- I_{PT} = indicator variable for pavement type (= 1.0 if concrete, 0.0 otherwise);
- I_{AG} = indicator variable for approach grade (= 1.0 if absolute grade \geq 0.5 percent, 0.0 otherwise); and
- L_C = curve length, ft.

Table 2. Curve Speed Models for Rural Multilane Highways.

Author(s)	Significant Variables*	Roadway Type	Data Measures	Measurement Tools
Gong and Stamatiadis (17)	ST, MT, PT, AG, Lc, FC, R	Four-lane rural	Spot speeds	Radar guns
Cheng et al. (18)	Δ , R of preceding curve, R of successive curve	Eight-lane expressway	Spot speeds	Radar guns
Montella et al. (19)	1/R, Gu, CCR2, tunnel, bridge, Lt, Rcb,	Four-lane divided (motorway)	Continuous speeds	Instrumented vehicle
Semeida (20)	MW, Δ , R	Multilane rural	Spot speeds	Radar guns
Morris and Donnell (21)	1/R, AG, LW, SW, e, posted speed limits for cars and trucks, curve deflection (left/right)	Multilane rural with >4% vertical grades on tangents	Continuous speeds	Laser guns

* ST = shoulder type, SW = shoulder width, LW = lane width, MT = median type, MW = median width, PT = pavement type, AG = approaching section grade, Lc = length of curve, FC = front of curve index, R = curve radius, Δ = deflection angle, e = superelevation rate, Gu = equivalent upgrade, CCR2 = curvature change ratio of 2 km preceding curve, Lt = length of tangent.

Cheng et al. published the models for passenger car and truck speeds on multilane highway curves that are described by Equations 7 and 8, respectively (18). These models apply to vehicles' average speeds along all points on the curve and include only an empirical constant and deflection angle.

$$v_{c,85,pc} = 80.5 - 0.126\Delta \quad (7)$$

$$v_{c,85,tk} = 46.36 + \frac{66.9}{\Delta} \quad (8)$$

where:

- $v_{c,85,pc}$ = 85th-percentile passenger car speed, mph; and
- $v_{c,85,tk}$ = 85th-percentile truck speed, mph.

Cheng et al. developed additional models to predict vehicle speeds at the curve point of curvature (PC), midpoint of curve (MC), and point of tangency (PT). Their model for curve PC speed included a term for the radius of the preceding curve, and their models for curve MC and PT speeds included a term for the radius of the following curve.

The models shown in Equations 5–8 appear to be purely empirical in form. It is likely that a theoretical construct like what was shown in Equations 1 and 2 would yield a more robust model form. The findings of Gong and Stamatiadis (17) show that it may be necessary to derive separate models for the two travel lanes on a multilane highway curve. The findings of Cheng et al. (18) show that different trends exist for passenger cars and trucks, which is consistent with the findings of Bonneson et al. (2) (see the I_{tk} term in Equation 3).

In Italy, Montella et al. (19) used an instrumented vehicle with GPS continuous speed tracking to analyze driver behavior relative to speed choice—deceleration or acceleration—to develop operating speed prediction models. The noise in their dataset was removed to analyze the continuous speed profile while the underlying patterns were preserved with a smoothing algorithm. This was done using the LOWESS algorithm. The data were collected on a four-lane rural motorway. Separate models were developed to predict the operating speeds for:

- Curves and tangents.
- Deceleration and acceleration rates.
- Starting and ending points of constant operating speed in a curve.
- 85th percentile of the deceleration and acceleration rates of individual drivers.
- 85th percentile of the individual drivers' maximum speed reduction in the tangent-to-curve transition.

The researchers found that speed parameters were affected by a single geometric element as well as the geometric characteristics of the route preceding the curve. They also found that drivers' speed was not constant along curves, individual drivers' maximum speed reduction was greater than the operating speed difference in the tangent-to-curve transition, and the deceleration and acceleration rates experienced by individual drivers were greater than the deceleration and acceleration rates used to draw operating speed profiles.

Semeida (20) collected and analyzed speed data on 78 curves on multilane highways. The analysis used regression models to investigate the relationships between 85th-percentile curve speed and horizontal alignment and roadway factors. The analysis developed separate speed models for cars and trucks. A second analysis used artificial neural networks (ANNs) to investigate the relationships from the first analysis. It was found that the ANN modeling yielded better speed predictions. The most influential variable on 85th-percentile curve speed for cars was the curve radius, whereas the median width was the most influential variable for trucks.

As part of National Cooperative Highway Research Program (NCHRP) Project 15-39, Morris et al. (21) collected speed data along 19 multilane highways in the states of Washington, California, West Virginia, Maryland, and Pennsylvania. All sites contained a tangent section with grades greater than 4 percent preceding a horizontal curve. They investigated the relationship between passenger car and truck speeds using a three-stage least-squares (3SLS) modeling approach to predict passenger car and truck operating speeds on multilane highways with combinations of horizontal curves and steep vertical grades. The mean operating speeds were modeled as a function of several geometric design features and the traffic control devices present at each site. The findings indicate that the curve radius has a larger influence on passenger car operating speeds than on truck speeds, but vertical grade seems to influence truck

operating speeds more significantly than passenger car speeds. Increasing the right shoulder width was associated with higher passenger car operating speeds, but the lane width was not statistically significant in the passenger car speed models. Increasing the lane width, however, was associated with higher truck operating speeds; the right shoulder width was not associated with truck operating speeds. An endogenous relationship between truck and passenger car operating speeds was found. Higher posted speed limits were also found with higher truck and passenger car operating speeds.

CURVE SAFETY TRENDS

Fitzpatrick et al. analyzed curve safety trends by categorizing curves in terms of speed reduction (22). They defined speed reduction as the difference between 85th-percentile vehicle speeds on the approach tangent and at the curve midpoint. They found that a curve requiring a 5-mph speed reduction is likely to have 90 percent more crashes than a tangent segment, and a curve requiring a 10-mph speed reduction is likely to have 250 percent more crashes. They calibrated the following crash modification factor (CMF) to estimate a relationship between curve crash frequency and the 85th-percentile curve and tangent speeds:

$$CMF_{sr} = e^{0.126(v_{t,85} - v_{c,85})} \quad (9)$$

where:

CMF_{sr} = crash modification factor for curve speed reduction.

The trend in Equation 9 shows that curve crash frequency increases exponentially as the required speed reduction increases.

Bonneson and Pratt calibrated a safety prediction model to estimate the effects of geometry and traffic operations on safety (23). The model was calibrated for rural highways using Texas data. It includes a CMF to account for the expected increase in crash frequency due to the presence of a horizontal curve. The following equation describes the horizontal curve CMF:

$$CMF_{cr} = 1.0 + 0.97(0.147V)^4 \frac{(1.47V)^2}{32.2R^2} \left(\frac{L_c}{L}\right) \quad (10)$$

where:

CMF_{cr} = crash modification factor for horizontal curve radius;

V = posted speed limit, mph;

L = segment length, ft.

The CMF is illustrated in Figure 2 for a range of curve radii and three posted speed limit values. Two trends are noticeable. First, crash frequency increases significantly when a curve of any radius is present, but especially if the curve radius is less than about 2000 ft. Second, a curve of a given radius will be associated with a larger increase in crashes if vehicle speeds are higher. For example, a curve with a radius of 2865 ft (i.e., degree of curve = 2.0) will be associated with

a crash frequency increase of about 6 percent ($CMF_{cr} = 1.06$) on a 50-mph roadway and about 44 percent ($CMF_{cr} = 1.44$) on a 70-mph roadway.

Lord et al. calibrated a model to predict the annual roadway departure crash frequency per mile on curves (7). This model suggests that crash frequency per mile increases exponentially with an increase in degree of curve (or a decrease in radius). This model is described as follows:

$$\mu = e^{-6.448} \times F^{0.7657} \times e^{(-0.076LW - 0.062SW + 0.075CD)} \quad (11)$$

where:

- μ = estimated annual number of crashes per mile;
- F = traffic volume, vehicles per day;
- LW = lane width, ft;
- SW = shoulder width, ft; and
- CD = degree of curve.

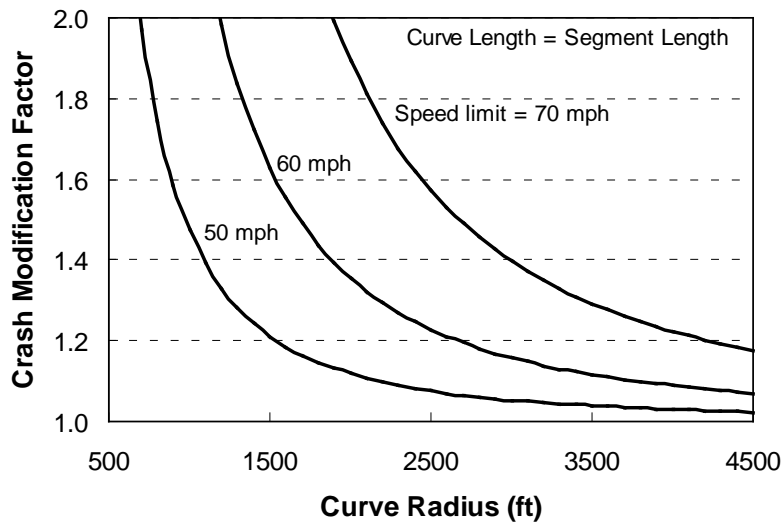


Figure 2. Curve Radius Crash Modification Factor.

Some studies have evaluated the effects of these traffic control devices on reducing horizontal curve-related crashes. Lalani (24) collected crash records one year before and after the installation of Chevrons at three sites in California. A naïve before-after comparison showed the crashes reduced by 64 percent in the after period (i.e., $CMF = 0.36$).

Srinivasan et al. obtained geometric, traffic, and crash data at 89 treated curves in Connecticut and 139 treated curves in Washington to determine the safety effectiveness of improved curve delineation (25). The researchers conducted an empirical Bayes (EB) before-after analysis to account for potential selection bias and regression-to-the-mean bias. Results revealed an 18.0 percent reduction in injury and fatal crashes, a 27.5 percent reduction in crashes during dark conditions, and a 25.0 percent reduction in lane departure crashes during dark conditions. The combined CMF , using meta-analysis, was 0.86. This CMF is a little higher than

that provided by TxDOT’s Work Code Table (i.e., 0.75). Srinivasan et al. conducted a further economic analysis. Results revealed that improving curve delineation with signing improvements is a very cost-effective treatment with the benefit-cost ratio exceeding 8:1. More recently, Choi et al. analyzed the safety effect of Chevrons on three freeways in Korea using an EB before-after study (26). Their estimated CMF for installing Chevron signs was 0.72, which is fairly close to the results found by Srinivasan et al.

Montella comprehensively evaluated the safety effectiveness of improving horizontal curve delineation (27). The researcher collected crash data at 15 curves in Italy and performed an EB before-after study. It was found that total, nighttime, daytime, rainy, non-rainy, run-off-road, and property-damage-only crashes reduced significantly after improving curve delineation. Specifically, total crashes reduced by about 39.4 percent. The most effective treatment was the installation of curve warning signs, Chevron signs, and sequential flashing beacons along the curve. The CMFs for these treatments are listed in Table 3.

Table 3. Curve Delineation CMFs.

Crash Type	CMF by Curve Delineation Treatment Type		
	Chevrons	Curve Warning Signs and Chevrons	Curve Warning Signs, Chevrons, and Beacons
Total	0.97	0.59	0.52
Nighttime	1.92	0.66	0.23
Daytime	0.63	0.56	0.63
Rainy	0.41	0.49	0.56
Non-rainy	1.27	0.69	0.48
Run-off-road	0.90	0.56	0.52
Non-run-off-road	1.29	0.76	0.53
Injury	1.46	1.18	0.62
Property-damage-only	0.83	0.46	0.44

Tsyganov et al. studied the safety effects of edgelines on rural two-lane highways (28). Their research found that edgelines on rural two-lane roadways may reduce crash frequency up to 26 percent, and the highest safety impacts occur on curved segments of roadways with lane widths of 9–10 ft. As such, the researchers estimated CMFs for installing edgeline markings on rural two-lane curves as 0.67 (for 9-ft-wide lanes) and 0.74 (for 9- to 11-ft lanes). Elvik and Vaa reviewed previous studies and provided the CMF for the Combination Horizontal Alignment and Advisory Speed sign as 0.87 (29).

DATA SIGNAL AND NOISE PROCESSING TRENDS

To obtain useful roadway measurement data from raw measurement device data streams, it is necessary to apply data processing methods such as filtering, smoothing, or polynomial fitting. For example, the TRAMS program applies a Kalman filter to raw heading change data from the GPS receiver, and then fits a sixth-order polynomial to the filtered data (3). The filtering and fitting concepts are shown in Figure 3 and Figure 4, respectively. Raw vehicle headings are measured by the GPS receiver and recorded by the TRAMS program. Heading changes between successive observations are computed for the purpose of obtaining the

deflection angle for the curve portion that was traversed during the corresponding time interval. A Kalman filter and a fitted polynomial are used to smooth the data to avoid spurious calculations due to data noise.

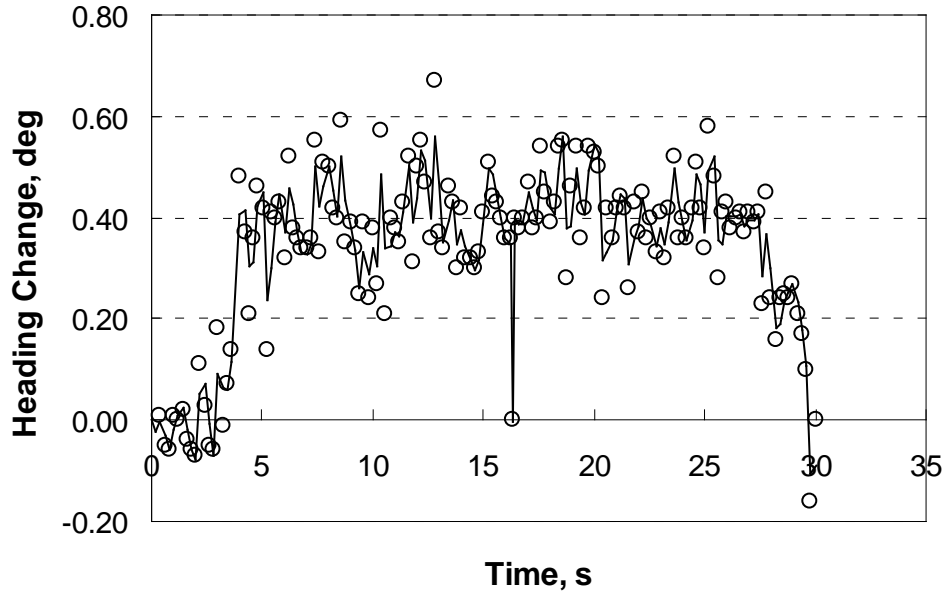


Figure 3. Raw and Kalman-Filtered Heading Change Data.

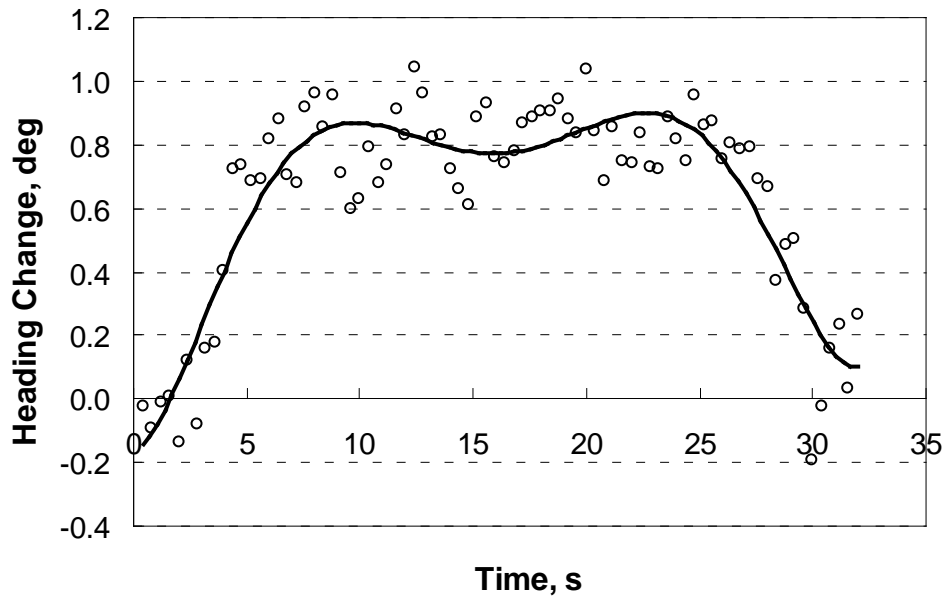


Figure 4. Aggregated Filtered Heading Change Data with Sixth-Order Polynomial.

Roadway measurements involving GPS receivers, accelerometers, inclinometers, or barometers (e.g., grade) would require the use of similar methods. In addition to the Kalman filter, pass filters can help eliminate extreme values. There are two types of pass filters. A high-pass filter (HPF) attenuates content below a cutoff frequency, allowing higher frequencies to pass through the filter. The amount of attenuation for each frequency depends on the filter design. An HPF can be used to differentiate between program signal and low-frequency noise. It is sometimes called a low-cut filter or bass-cut filter. A low-pass filter (LPF) attenuates content above a cutoff frequency, allowing lower frequencies to pass through the filter. An LPF can be used to eliminate unwanted and counterproductive bandwidth. The LPF is sometimes called a high-cut filter, or treble-cut filter. When an HPF is used in conjunction with an LPF, a band-pass filter is produced. A band-pass filter is a device that passes frequencies within a certain range and rejects (attenuates) frequencies outside that range. Pass filters are useful in reducing or eliminating the offending signal content.

Pass filters have been used for various applications in transportation engineering. For example, Gillespie showed that the spatial power spectral density of a typical road surface has a low-pass characteristic, which decreases at the increase of the spatial frequency (30). In considering this characteristic, various studies modeled the road elevation profile as white Gaussian noise filtered by a first-order LPF (30, 31). For the prediction of road traffic noise, Iwase et al. (32) used a power spectral model filtered by a first-order LPF with a defined cutoff frequency. Karamihas et al. (33) developed guidelines for pavement profile measurement, in which they used a two-pole Butterworth LPF for the accelerometer and height sensor signals. The Profile Viewing and Analysis (ProVAL) software that is used to view and analyze pavement profiles has the Butterworth filter set with band-pass filtering (www.RoadProfile.com). The band-pass filtering option applies the HPF with the requested long-wavelength cutoff, and then the LPF with the requested short-wavelength cutoff.

In an attempt to construct indicators of regional economic activity based on local traffic intensity data, van Ruth (34) used vehicle flow data from traffic sensors. The author used the Butterworth filter as an LPF to remove some of the observation-to-observation noise of the individual sensors. For the traffic incident detection using videos, Liu et al. (35) noted that most of the image energy is concentrated in the low-frequency and medium-frequency bands in the amplitude spectrum, while in the high-frequency band, important information is often overwhelmed by noise. The study used Gaussian LPFs to weaken the impact of high-frequency noise.

As opposed to parametric methods (i.e., typically regression analyses that use a dataset to estimate the parameters of certain families of models), non-parametric methods do not constrain the data to follow a family of curves with prescribed shapes and distribution moments. Rather, these methods look at the signal locally, trying to minimize the error of the fitted curve within certain proximity of each point in the series. This method is achieved by estimating a fitted value that is influenced by its neighboring points, with such influence decreasing inversely with the distance to the fitting point. As a result, the data stream trend can be represented more clearly and without assumptions about its functional form. An analyst can then recognize trends and either perform statistical analysis on the filtered curve or postulate appropriate functional forms for further parametric statistical analysis.

The following scenario illustrates the use of non-parametric methods in a scenario similar to the proposed scope of work in this project. The subject of study is a speed profile of a vehicle traveling at 60 mph from $t = 0$ seconds to $t = 4$ seconds, smoothly decelerating to 40 mph from $t = 4$ seconds to $t = 8$ seconds, and traveling at 40 mph from $t = 8$ seconds to $t = 10$ seconds. However, this speed profile is measured with an electronic device that generates a noisy signal recorded with a rate of 25 Hz. It is known that a speed point from this signal deviates from the actual speed by 2.5 mph on average. The raw data from this device are shown in black in Figure 5, and the actual speed is shown as a blue dashed line for comparison.

A smoother non-parametric curve fitted to the raw data is shown in red. The smoother curve fits the data well, following very closely the blue ground-truth signal. Statistics from the fitted curve were obtained to estimate the amount of error that can be attributed to signal noise: a mean absolute error of 2.529 mph compares closely to the real mean absolute error (as previously known from the device) of 2.5 mph.

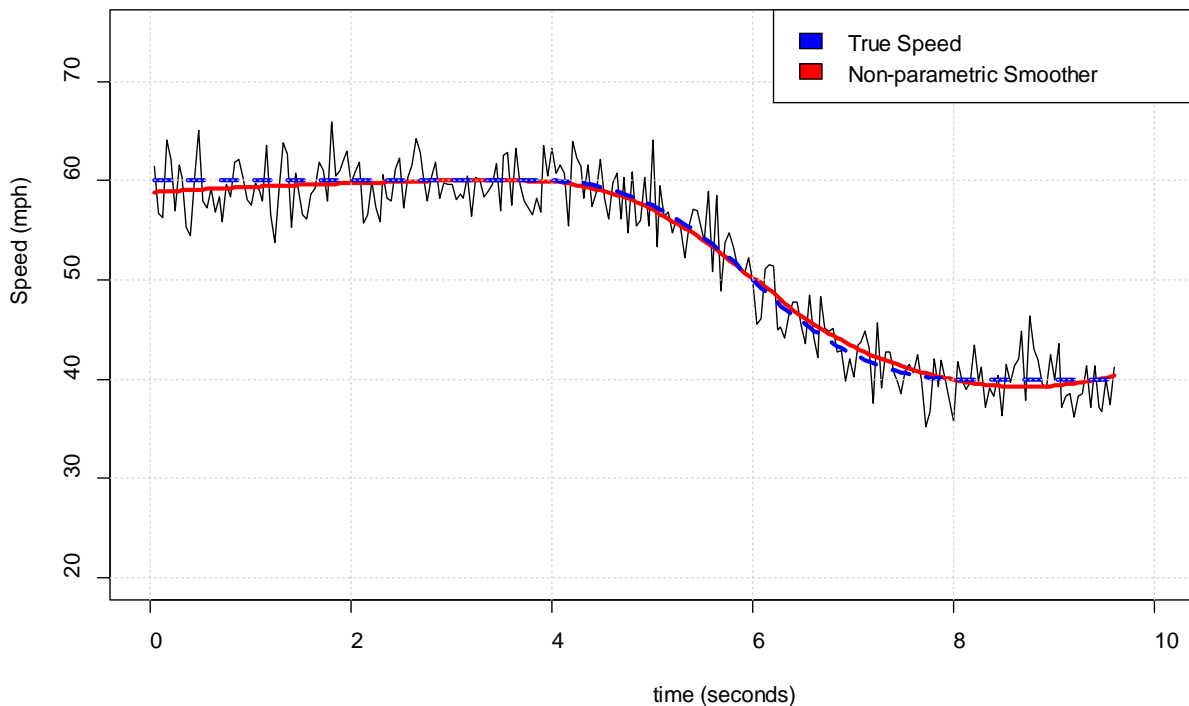


Figure 5. Example of Smoothing Curve on a Noisy Speed Signal.

The performance of the smoother curve is appropriate in this example, and it can safely be considered a good approximation of the blue line. In a realistic scenario, the blue line is unknown, but the non-parametric line can be obtained from the raw signal and used as a viable approximation of the true speed profile. This technique has been used in the past with promising results (36).

The non-parametric method shown in Figure 5 is known as the LOWESS smoother. This method develops a curve that follows the scatterplot with no assumptions about the functional form of the whole curve (i.e., linear, quadratic, polynomial, etc.). The name of this procedure

originally stood for “Locally Weighted Scatterplot Smoother.” Although it is widely used as a smoother and a filter, it has been expanded to incorporate multiple covariates and is now generally considered a modeling tool, given some useful statistical properties (37). It is called local regression because each fitted point is estimated from the data available within a preset span (this span may be varied depending on the frequency rate of the data, total length of signal series, and other considerations). Typically, the procedure fits a series of quadratic polynomials used in regular intervals for subsequent spans of the overall dataset (as in Figure 5), but higher-order polynomials can be used. The balance between bias and variance is adjusted by changing the span interval length and the polynomial degree, adjusting how localized the fit of the smoother function is. If the smoother is too localized, then the resulting curve over-fits the data and retains a large proportion of noise. In this case, an analyst will underestimate the signal noise from this curve. On the contrary, if the smoother is not localized enough, it will lose information and will tend to exhibit bias at locations where inflections in the signal occur.

CHAPTER 3: CURVE SPEED DATA COLLECTION AND ANALYSIS

INTRODUCTION

This chapter describes data collection activities that were undertaken to provide quantitative information about the influence of horizontal curve geometry and traffic control characteristics on vehicle speeds. The insights gained from the cross-sectional analysis of speeds were used to extend existing guidelines for setting curve advisory speeds.

The chapter is divided into three parts. The first part describes the procedures that were used to identify sites and collect vehicle speed data on curves with a range of site characteristics. The second part presents a summary of the operational dataset. The third part presents the calibrated speed prediction models.

SPEED DATA COLLECTION PLAN

This part of the chapter describes the plan to identify sites and collect curve speed data.

Database Attributes

The curve speed database includes the following attributes for vehicles traversing horizontal curves:

- Vehicle speed on the approach tangent (TN).
- Vehicle speed at the MC.
- Headway (leading and trailing).
- Vehicle classification (car or truck).

Vehicle speeds at the MC represented the dependent variables in the models to be developed. Approach tangent speed and vehicle classification were collected because they have been found to be important predictors of curve speed (2). Headways were collected because the models were to be calibrated to describe the behavior of free-flowing vehicles. Thus, it was necessary to identify only free-flowing vehicles for inclusion in the model calibration dataset.

Additionally, attributes to describe the data collection sites were recorded. These attributes are listed in Table 4, along with the desired ranges for the attributes. A site was defined as one direction of travel on a horizontal curve. Thus, if data were collected in both travel directions on a curve, the curve provided two data collection sites.

Radius, deflection angle, superelevation rate, grade, lane width, and shoulder width were included in the speed models as appropriate. Ranges in the site attributes were sought to ensure that the calibrated speed models would be transferable to a range of site conditions. In particular, ranges in the attributes of radius, regulatory speed limit, and speed reduction were essential to ensure that both gradual and severe curves were included in the calibration dataset.

Table 4. Site Description Data.

Variable	Basis	Range Among Sites
Curve radius	Site	700 to 5300 ft
Deflection angle	Site	7 to 80 degrees
Spiral transition presence	Site	None present
Regulatory speed limit	Site	55 to 75 mph
Speed reduction (regulatory – advisory)	Site	0 to 30 mph
Superelevation rate	MC	0 to 14 percent
Grade	TN, MC	-5.7 to +6.0 percent
Lane width	MC	10.5 to 13.8 ft
Shoulder width	MC	0 to 12 ft

Data Collection Methods

The data collection sites were chosen using preliminary information available in the Texas Reference Marker (TRM) database and aerial photography, with the goal of achieving a range in the variables listed in Table 4. Preliminary data collection occurred in the office. Then, the sites were visited to conduct a field survey and deploy the equipment needed to collect the speed data.

Preliminary Data

The TRM database was queried to develop a list of data collection sites. The data extracted from TRM included degree of curve (which can be used to compute radius), deflection angle, regulatory speed limit, ADT, lane width, and shoulder width. When possible, the Street View imagery available in Google Earth was used to verify the regulatory speed data obtained from TRM. The Street View imagery was also used to obtain the curve advisory speed and determine the presence of supplemental traffic control devices, like delineator posts and Chevrons, and presence of marked edgelines and longitudinal barriers.

Site Survey

The site survey task was to hand-measure lane width, shoulder width, superelevation rate (or cross slope), and grade. These measurements were taken on the approach tangent and at the MC. Width measurements were taken using a measuring wheel. Superelevation and grade measurements were taken using a smart level.

Speed Data

Vehicle speeds were collected using either side-fire radar or traffic classifiers with pneumatic tubes. These data were collected at the approach tangent and the MC. Where possible, traffic classifiers and tubes were used, but it was often necessary to use side-fire radar because traffic volumes and/or speeds were too high to allow tubes to be deployed safely, or traffic and pavement conditions made it difficult to keep the tubes secured for a sufficient time period. Ideally, the speed traps in the curves were located at the MC. However, site conditions sometimes required the locations of the traps to be adjusted (e.g., if there was a driveway located

near the ideal trap location). The MC trap was located within the zone that represented 45–55 percent of the curve’s length.

The approach tangent trap was located such that the free-flow speeds of vehicles could be observed. Locations were identified where drivers had likely not yet started to decelerate because of the curve, using the following equation:

$$D_{min} = 1.47t_{pr}(v_{SL} + 5) + 1.47^2 \frac{(v_{SL} + 5)^2 - (v_{ADV} + 5)^2}{2d_r} \quad (12)$$

where:

- D_{min} = minimum distance from curve PC to approach tangent speed trap, ft;
- t_{pr} = 85th-percentile perception-reaction time (use 1.0 sec), sec;
- v_{SL} = regulatory speed limit, mph;
- v_{ADV} = posted advisory speed, mph; and
- d_r = deceleration rate (use 3.3 ft/s²), ft/s².

The regulatory speed limit and advisory speed were increased by 5 mph to reflect a conservative estimate of the 85th-percentile approach tangent and curve midpoint speeds.

Site Selection and Screening

A query of the TRM database was conducted to identify curves with characteristics that fit within the ranges described in Table 4 (with the exception of superelevation rate, which is not included in the TRM database). To minimize travel time during data collection activities, the query was limited to the TxDOT districts of Bryan, Waco, Lufkin, San Antonio, Austin, Fort Worth, and Dallas. This query yielded 1541 candidate curves for further screening.

The candidate curves were weighted and prioritized using the attributes in the TRM database, particularly curve length and radius. High priority was given to curves with radii less than 1500 ft due to the paucity of curves on four-lane highways with radii in this range. The sites were further screened by using aerial and street-level photography available in Google Earth and Google Street View. The screening process was conducted to check for paved driveways, crossroad approaches, or entrance or exit ramps on the curve or within the approach tangent area to verify that the curve was isolated from other curves (such that free-flow vehicle speeds could be measured on the approach tangent), and to see if the curve was located close enough to a town that vehicle speeds would likely not reflect free-flow conditions. The list of candidate curves was reduced to about 30 curves for more detailed evaluation.

DATA SUMMARY

This part of the chapter presents the results of the data collection efforts, including a description of the sites and a preliminary analysis of the operational dataset.

Data Collection Site Characteristics

A total of 23 curves were ultimately selected for data collection. Table 5 provides descriptions of the data collection site locations and traffic control characteristics. The travel direction indicates the direction that vehicles turned while traversing the data collection site. The geographic distribution of the sites is shown in Figure 6.

Table 5. Site Location and Traffic Control Characteristics.

Functional Classification	Curve Number	Travel Direction	Posted Speed, mph		Highway	ADT, veh/d (2012)	Delineation Treatments
			Regulatory	Advisory			
2U	5063	L	75	None	FM 107	1234	None
	5070	L	75	None	FM 107	1204	None
	63049	L, R	75	45	SH 16	903	None
	89356	L, R	75	None	SH 7	2600	None
4D	62315	R	75	None	SH 6	15,470	None
	64908	L	60	None	SH 31	9390	None
	68640	L, R	65	None	SH 101	9257	Delineators
	78307	L	65	None	US 80	8374	None
	89126	L, R	75	None	SH 6	9731	Delineators
	89159	R	60	None	US 380	18,496	Delineators
	89163	L, R	70	None	US 380	18,892	None
4F	53311	R	80	None	IH 10	11,673	None
	53319	R	80	None	IH 10	12,472	None
	53324	L, R	75	None	IH 10	12,472	Delineators
	53819	L, R	75	None	IH 20	19,330	None
	53831	L, R	65	None	IH 20	31,124	Delineators
	81722	L, R	70	None	SH 6	18,120	None
4U	62595	L, R	75	None	SH 7	5624	None
	64294	L, R	60	50	SH 21	3604	Chevrons
	64692	L, R	55	None	SH 29	5715	Chevrons
	64719	L, R	65	None	SH 29	5865	None
	64738	L, R	55	None	SH 29	12,117	Delineators
	83517	L, R	70	65	US 290	3685	None

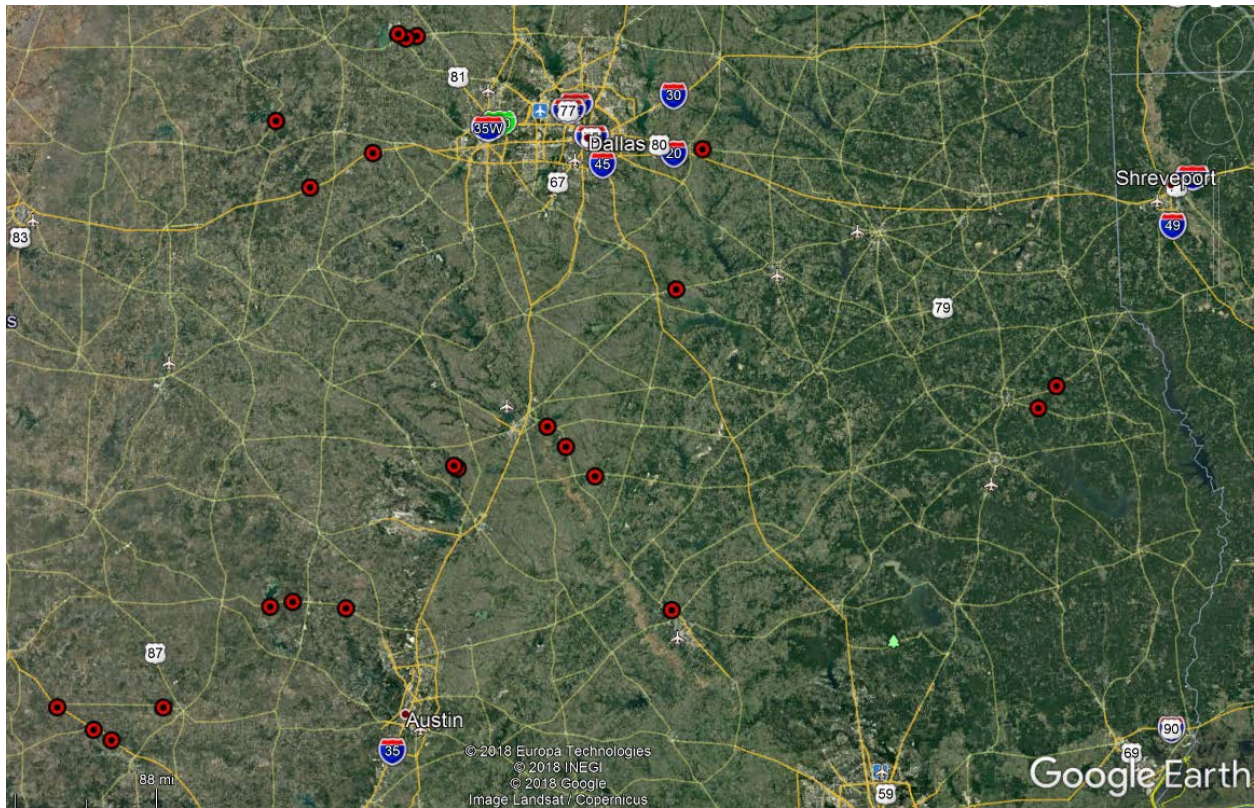


Figure 6. Speed Data Collection Site Locations.

Site geometric characteristics are provided in Table 6. The deflection angle values were extracted from aerial photographs and the TRM database. The radius values were computed from the deflection angles and curve lengths that were measured from aerial photographs.

Pavement measurements, including superelevation rate at the MC speed trap, cross slope at the TN trap, and vertical grades at both traps, are provided in Table 7. On the approach tangent, the typical cross slope of 2 percent was defined as positive for curves deflecting to the right and negative for curves deflecting to the left. Within the curve, superelevation was defined as positive if its direction contributed to an increase in side friction supply (i.e., sloped downward to the right for right-deflecting curves or to the left for left-deflecting curves). Grade was measured on the shoulder and was defined as positive or negative based on the direction of travel.

Table 6. Site Geometric Characteristics.

Functional Classification	Curve Number	Travel Direction	Radius, ft	Deflection Angle, degrees	Cross-Sectional Width, ft		
					Left Shoulder	Lanes (total)	Right Shoulder
2U	5063	L	1866	35	0.0	11.5	10.0
	5070	L	2196	34	0.0	11.0	11.0
	63049	R	711	80	0.0	13.8	0.0
	63049	L	711	80	0.0	11.8	0.0
	89356	R	2849	36	0.0	11.0	11.5
	89356	L	2849	36	0.0	11.0	12.0
4D	62315	R	2518	40	7.0	24.0	9.0
	64908	L	2787	14	3.0	23.5	7.4
	68640	R	1793	42	4.4	23.8	9.8
	68640	L	1793	42	3.6	24.3	8.9
	78307	L	2120	22	2.5	23.6	10.5
	89126	R	1896	40	5.0	24.0	12.0
	89126	L	1896	40	5.0	24.0	12.0
	89159	R	2636	24	3.5	23.9	9.8
	89163	R	2848	14	7.2	23.2	9.6
89163	L	2848	14	6.1	23.8	9.7	
4F	53311	R	4725	15	11.5	24.2	3.4
	53319	R	3413	7	4.2	23.6	10.3
	53324	R	2821	25	4.5	24.4	10.0
	53324	L	2821	25	4.2	24.1	9.1
	53819	R	5316	27	10.0	24.0	14.0
	53819	L	5316	27	10.0	24.7	15.0
	53831	R	3358	18	12.1	24.0	14.0
	53831	L	3861	18	10.1	24.5	15.7
	81722	R	3599	48	5.0	24.0	11.0
81722	L	3599	48	4.5	24.0	11.0	
4U	62595	R	1891	14	0	22.0	3.0
	62595	L	1891	14	0	22.0	1.0
	64294	R	865	38	0	23.0	4.0
	64294	L	865	38	0	23.0	4.0
	64692	R	1047	33	0	23.5	4.0
	64692	L	1047	33	0	23.5	4.0
	64719	R	1372	41	0	23.0	3.0
	64719	L	1372	41	0	23.0	3.0
	64738	R	1787	32	0	21.0	2.0
	64738	L	1787	32	0	21.0	2.0
	83517	R	1312	43	0	23.0	4.0
83517	L	1312	43	0	21.5	6.0	

Speed Data Preliminary Analysis

Speed measurement equipment was deployed at each data collection site for at least 24 hours to obtain both daytime and nighttime measurements and to ensure that a sufficient

number of trucks would be observed. In total, about 1,080,000 vehicles were observed. The distribution of these vehicles across the sites and speed traps is shown in Table 8.

Table 7. Site Pavement Characteristics.

Functional Classification	Curve Number	Travel Direction	Cross Slope, %	Superelevation Rate, %	Vertical Grade, %	
					TN	MC
2U	5063	L	0.9	2.8	0.5	1.0
	5070	L	-0.5	2.9	0.4	0.6
	63049	R	0.6	3.7	0.9	1.3
	63049	L	1.2	0.0	4.4	0.6
	89356	R	0.7	2.6	-2.2	-0.5
	89356	L	-0.2	3.0	-0.4	0.4
4D	62315	R	0.9	5.8	-0.7	-0.5
	64908	L	2.2	2.5	1.9	0.8
	68640	R	1.9	6.8	1.2	0.7
	68640	L	2.4	6.0	0.1	0.5
	78307	L	1.9	8.2	0.3	2.9
	89126	R	3.1	6.7	1.7	-0.6
	89126	L	-1.3	6.7	0.4	0.4
	89159	R	2.2	5.9	0.9	2.8
	89163	R	2.1	7.2	1.8	2.4
	89163	L	0.5	3.4	0.6	1.6
4F	53311	R	2.1	4.1	-0.3	-0.7
	53319	R	-1.6	4.2	-1.7	-1.9
	53324	R	3.6	-6.5	1.1	-1.0
	53324	L	-2.1	6.7	-0.3	1.0
	53819	R	2.1	3.3	1.0	0.5
	53819	L	-1.5	3.1	-0.9	-0.7
	53831	R	1.4	4.9	1.1	3.1
	53831	L	-2.0	4.3	-1.3	-2.6
	81722	R	-0.7	4.2	1.0	0.4
	81722	L	2.4	5.2	-0.5	-0.8
4U	62595	R	-1.0	5.9	-3.5	-5.7
	62595	L	-2.1	6.8	-5.6	6.0
	64294	R	-2.4	5.8	-1.0	1.8
	64294	L	-1.9	6.0	0.6	1.7
	64692	R	6.3	11.1	-2.4	4.0
	64692	L	-0.5	8.2	-1.7	-3.9
	64719	R	-3.1	7.6	-0.9	-1.1
	64719	L	-2.6	9.0	0.5	1.8
	64738	R	-1.9	6.9	-1.4	0.5
	64738	L	-1.9	6.6	-1.7	-0.7
	83517	R	2.0	12.0	1.7	1.1
	83517	L	-1.4	10.0	1.8	-0.9

The modeling dataset included a subset of the total vehicle sample. Vehicles were discarded from the dataset for the following reasons:

- The vehicle was not observed at both speed trap locations.
- The vehicle changed lanes between locations.
- The vehicle’s length measurements, axle counts, or vehicle classification numbers differed notably between locations.
- The vehicle was not classified as “free-flow” (i.e., its headways were less than 7 seconds at one or both locations).
- The vehicle was observed with a higher speed at the MC location than at the TN location, suggesting that the driver’s speed choice was likely influenced by factors other than the curve geometry.

Table 8. Vehicle Counts by Site.

Functional Classification	Curve Number	Travel Directions	Number of Vehicles Observed			
			TN speed trap		MC speed trap	
			L	R	L	R
2U	5063	L	880	—	841	—
	5070	L	981	—	927	—
	63049	L, R	1357	1156	1282	1316
	89356	L, R	2031	2224	2026	2202
4D	62315	R	—	15,057	—	15,615
	64908	L	14,446	—	20,608	—
	68640	L, R	18,046	16,585	13,721	20,305
	78307	L	25,999	—	27,599	—
	89126	L, R	11,028	9904	11,320	30,758
	89159	R	—	9973	—	9391
	89163	L, R	17,100	24,232	26,770	28,343
4F	53311	R	—	11,990	—	11,882
	53319	R	—	12,989	—	13,019
	53324	L, R	15,500	10,904	11,976	34,629
	53819	L, R	15,981	18,670	43,806	18,237
	53831	L, R	23,182	23,138	62,880	22,483
	81722	L, R	30,004	29,526	81,579	27,858
4U	62595	L, R	3495	3381	2787	7692
	64294	L, R	2807	2556	3061	7108
	64692	L, R	5139	4861	2537	4863
	64719	L, R	3437	5963	5386	6377
	64738	L, R	16,136	16,347	46,100	15,883
	83517	L, R	3091	2902	2970	2893

Additionally, an examination of the data from sites 64692L, 64719L, and 83517R revealed significant portions of time (i.e., multiple consecutive hours) where all vehicles were observed in only one of the two lanes. The speed data at these three sites were collected using tube sensors in a four-tube configuration to determine the lane used by each vehicle. Since no lane closures occurred during data collection, these observations are likely attributable to tube sensor ruptures. (For example, it is unlikely that hundreds of drivers over a period of 4 hours would all randomly choose to use the left lane on their side of the highway.) As a result, data from these three sites had to be discarded. The reduced count of vehicles used for statistical modeling efforts is provided in Table 9.

Table 9. Matched Free-Flow Vehicles by Site.

Functional Classification	Curve Number	Travel Direction	Number of Vehicles Observed				
			Total	Daytime		Nighttime	
				Car	Truck	Car	Truck
2U	5063	L	596	497	50	46	3
	5070	L	188	159	13	14	2
	63049	L	644	552	34	53	5
	63049	R	854	700	79	67	8
	89356	L	1032	745	155	100	32
	89356	R	1066	793	155	88	30
	All 2U sites		4380	3446	486	368	80
4D	62315	R	1730	1065	220	321	124
	64908	L	270	236	14	19	1
	68640	L	4749	2270	1407	439	633
	68640	R	4073	2113	1217	312	431
	78307	L	4274	3340	207	700	27
	89126	L	1493	876	241	257	119
	89126	R	456	311	58	70	17
	89159	R	1431	830	182	249	170
	89163	L	50	38	2	5	5
	89163	R	3621	2229	469	580	343
	All 4D sites		22,147	13,308	4017	2952	1870
4F	53311	R	1330	500	237	383	210
	53319	R	1348	552	304	282	210
	53324	L	2032	837	622	389	184
	53324	R	1884	941	263	277	403
	53819	L	985	201	186	189	409
	53819	R	1100	454	332	133	181
	53831	L	1384	503	209	313	359
	53831	R	1657	527	255	350	525
	81722	L	3426	1759	467	780	420
	81722	R	2673	1352	422	510	389
	All 4F sites		17,819	7626	3297	3606	3290
4U	62595	L	608	386	48	151	23
	62595	R	690	477	52	134	27
	64294	L	590	452	43	86	9
	64294	R	683	501	55	122	5
	64692	L	0	0	0	0	0
	64692	R	1841	1559	89	174	19
	64719	L	0	0	0	0	0
	64719	R	866	697	53	103	13
	64738	L	1180	813	50	291	26
	64738	R	1720	1140	130	410	40
	83517	L	255	226	4	21	4
	83517	R	0	0	0	0	0
	All 4U sites		8433	6251	524	1492	166

MODEL CALIBRATION

The researchers calibrated a total of nine speed models. The matrix of roadway characteristics and speeds is shown in Table 10. The researchers also used regression analysis to derive empirical relationships between daytime and nighttime speeds and passenger cars and trucks. In all cases, the researchers used the NLIN procedure in the Statistical Analysis Software (SAS) program (38).

Table 10. Model Calibration Matrix.

Roadway Configuration	Regulatory Speed Limit, mph	Speed Trap Location	Light Condition	Vehicle Type	Predicted Speed
2U	75	TN	Day	Car	85 th %
2U	75	MC	Day	Car	85 th %
2U	75	MC	Day	Car	Average
2U	75	MC	Day	Truck	85 th %
2U	75	MC	Day	Truck	Average
4U	55–75	TN	Day	Car	85 th %
4U	55–75	MC	Day	Car	85 th %
4U	55–75	MC	Day	Car	Average
4U	55–75	MC	Day	Truck	85 th %
4U	55–75	MC	Day	Truck	Average
4D & 4F	60–80	TN	Day	Car	85 th %
4D & 4F	60–80	MC	Day	Car	85 th %
4D & 4F	60–80	MC	Day	Car	Average
4D & 4F	60–80	MC	Day	Truck	85 th %
4D & 4F	60–80	MC	Day	Truck	Average

Two-Lane Undivided Highways with 75-mph Regulatory Speed Limits

The functional form for the approach tangent speed model was adopted from the analysis conducted by Bonneson et al. (2). It is described as follows:

$$V_{t,85,pc} = b_0 \sqrt{V_{sl}} (1 - e^{b_1(R+100)/5730}) \quad (13)$$

where:

- $V_{t,85,pc}$ = 85th-percentile passenger car speed at the approach tangent, mph;
- V_{sl} = regulatory speed limit, mph;
- R = curve radius, ft; and
- b_n = calibration coefficients.

The results of the calibration are shown in the left portion of Table 11. The numbers in the right portion of Table 11 are from the calibration documented by Bonneson et al. (2) for two-lane highways with regulatory speed limits of ≤ 70 mph. As shown, the intercept coefficient (b_0) is similar but the coefficient for radius (b_1) differs. The difference in radius coefficients is likely a reflection of the more gradual curve radii that were present on the 75-mph roadways used to calibrate the new model described herein.

Table 11. Approach Tangent Speed Model Calibration Results for Two-Lane Highways.

Model Statistics						
		Proposed			Bonneson et al. (2)	
R^2		0.88			0.69	
RMSE, mph		2.0			2.8	
Observations		6 sites (3446 passenger cars)			41 sites (6677 passenger cars)	
Range of Model Variables						
Variable	Variable Name	Units	Minimum	Maximum	Minimum	Maximum
V_{sl}	Regulatory Speed Limit	mph	75	75	55	70
R	Radius of Curve	ft	711	2849	318	1432
Calibrated Coefficient Values						
Coefficient	Coefficient Definition	Value	Std. dev	t-statistic	Value	Std. dev
b_0	Intercept	9.15	0.12	79.1	8.57	0.08
b_1	Effect of Radius	-13.29	0.92	-14.5	-35.21	3.59

The calibrated model is provided in Equation 14. A comparison of predicted and observed tangent speed values for the proposed model is provided graphically in Figure 7, and an additional examination of model fit for the two models is summarized in Table 12.

$$V_{t,85,pc} = 9.15\sqrt{V_{sl}}(1 - e^{-13.29(R+100)/5730}) \quad (14)$$

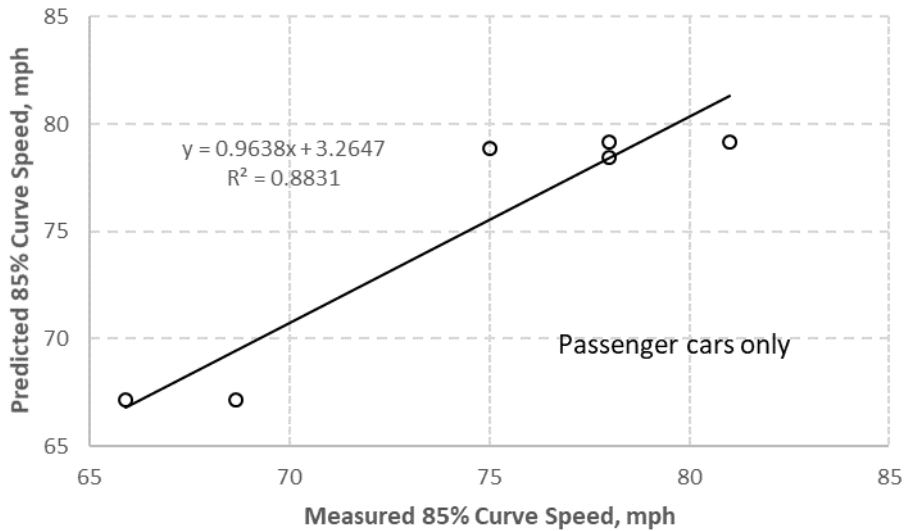


Figure 7. Comparison of Measured and Predicted Approach Tangent Speeds for Two-Lane Highways.

Table 12. Two-Lane Highway Approach Tangent Speed Model Predictions.

Measured Speed, mph	Predicted Speed, mph	
	Proposed	Bonneson et al. (2)
78.00	78.43	74.22
75.00	78.87	74.22
65.91	67.18	73.71
68.41	67.18	73.71
78.00	79.17	74.22
81.00	79.17	74.22

The functional form for the curve speed model was adopted from the analysis conducted by Bonneson et al. (2). It is described as follows:

$$v_c = \sqrt{\frac{15.0R_p \left(b_0 - b_1(1.47v_t) + 0.001b_2(1.47v_t)^2 + b_3I_{tk} + \frac{e}{100} \right)}{1 + 0.0322R_p b_2}} \leq v_t \quad (15)$$

The results of the calibration are shown in the left portion of Table 13 and Table 14. The numbers in the right portion of Table 13 and Table 14 are from the calibration documented by Bonneson et al. for two-lane highways with regulatory speed limits of ≤ 70 mph. Table 13 provides the estimates for the 85th-percentile curve speed, and Table 14 provides the estimates for average curve speed. In most cases, the coefficients in the proposed model and the model documented by Bonneson et al. are similar.

Table 13. 85th Percentile Curve Speed Model Calibration Results for Two-Lane Highways.

Model Statistics		Proposed			Bonneson et al. (2)		
R^2		0.98			0.97		
RMSE, mph		1.5			1.5		
Observations		47 sites (10,123 passenger cars, 2227 trucks)			41 sites (6677 passenger cars, 1741 trucks)		
Range of Model Variables							
Variable	Variable Name	Units	Min	Max	Units	Min	Max
V_t	Tangent speed	mph	58	81	mph	58	75
V_c	Curve speed	mph	39	79	mph	39	70
R	Radius of curve	ft	318	2849	ft	318	1432
I_c	Curve deflection angle	degrees	18	90	degrees	18	90
e	Superelevation rate	%	0	13.1	%	1.4	13.1
Calibrated Coefficient Values							
Coefficient	Coefficient Definition	Value	Std. dev	t-stat	Value	Std. dev	t-stat
b_0	Intercept	0.2866	0.0587	4.9	0.1962	0.0501	3.9
b_1	Effect of tangent speed	0.00137	0.0005	2.7	0.00072	0.0005	1.5
b_2	Effect of speed reduction	0.0412	0.0034	12.1	0.0338	0.0031	11.0
b_3	Effect of truck	-0.0198	0.0081	-2.4	-0.0150	0.0079	-1.9

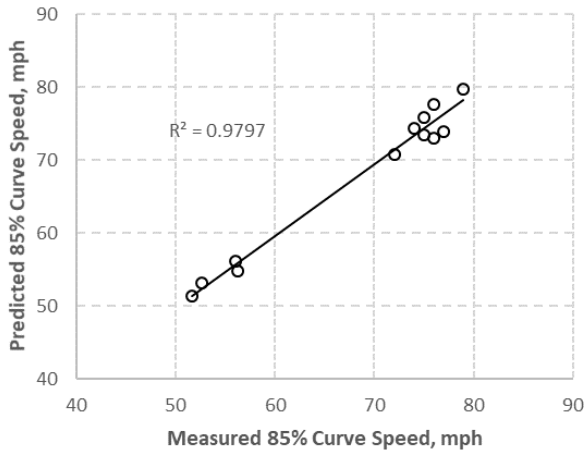
Table 14. Average Curve Speed Model Calibration Results for Two-Lane Highways.

Model Statistics		Proposed			Bonneson et al. (2)		
	R^2	0.99			0.98		
	RMSE, mph	1.0			1.2		
	Observations	47 sites (10,123 passenger cars, 2227 trucks)			41 sites (6677 passenger cars, 1741 trucks)		
Range of Model Variables							
Variable	Variable Name	Units	Min	Max	Units	Min	Max
V_t	Tangent speed	mph	58	81	mph	58	75
V_c	Curve speed	mph	39	79	mph	39	70
R	Radius of curve	ft	318	2849	ft	318	1432
I_c	Curve deflection angle	degrees	18	90	degrees	18	90
e	Superelevation rate	%	0	13.1	%	1.4	13.1
Calibrated Coefficient Values							
Coefficient	Coefficient Definition	Value	Std. dev	t-stat	Value	Std. dev	t-stat
b_0	Intercept	0.1920	0.0419	4.6	0.1118	0.0398	2.8
b_1	Effect of tangent speed	0.00082	0.0004	2.1	0.00045	0.0004	1.1
b_2	Effect of speed reduction	0.0464	0.0034	13.7	0.0423	0.0031	13.8
b_3	Effect of truck	-0.0129	0.0058	-2.2	-0.0108	0.0062	-1.8

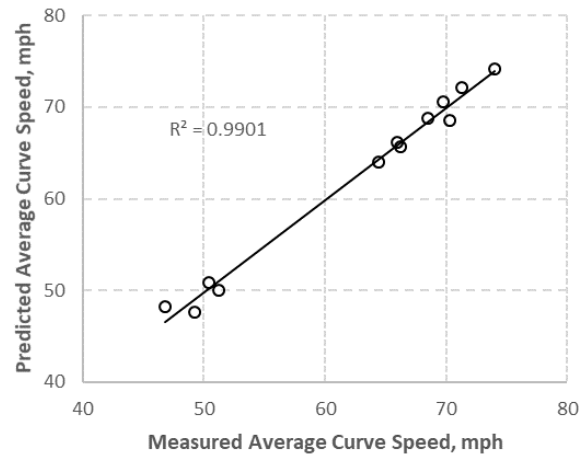
The calibrated models are provided in Equations 16 and 17. A comparison of predicted and observed tangent speed values for the proposed models is provided graphically in Figure 8, with each site represented by one data point for passenger car speeds and another point for truck speeds. An additional examination of model fit for the two models is summarized in Table 15.

$$v_{c,85} = \sqrt{\frac{15.0R_p \left(0.2866 - 0.00201v_{t,85} + 0.000089v_{t,85}^2 - 0.0198I_{tk} + \frac{e}{100} \right)}{1 + 0.00133R_p}} \leq v_{t,85} \quad (16)$$

$$v_{c,a} = \sqrt{\frac{15.0R_p \left(0.192 - 0.00121v_{t,a} + 0.0001v_{t,a}^2 - 0.0129I_{tk} + \frac{e}{100} \right)}{1 + 0.00149R_p}} \leq v_{t,a} \quad (17)$$



a. 85th-Percentile Speed



b. Average Speed

Figure 8. Comparison of Measured and Predicted Curve Speeds for Two-Lane Highways.

Table 15. Two-Lane Highway Curve Speed Model Predictions.

85 th -Percentile Speed			Average Speed		
Measured Speed, mph	Predicted Speed, mph		Measured Speed, mph	Predicted Speed, mph	
	Proposed	Bonneson et al. (2)		Proposed	Bonneson et al. (2)
77.0	73.9	72.2	70.3	68.6	65.8
72.0	70.8	69.2	66.2	65.7	62.8
75.0	73.5	71.9	66.0	66.2	63.2
76.0	73.0	71.6	64.5	64.0	61.0
56.3	54.7	51.9	51.2	50.1	46.8
51.6	51.3	48.5	49.2	47.7	44.3
56.0	56.1	53.3	50.4	50.9	47.7
52.6	53.1	50.4	46.8	48.3	45.0
76.0	77.7	76.5	71.3	72.1	69.5
74.0	74.5	73.3	68.5	68.8	66.0
79.0	79.8	78.6	74.0	74.2	71.7
75.0	75.8	74.7	69.8	70.5	67.9
RMSE	1.5	2.9	RMSE	1.0	3.2

For two-lane highways with 75-mph regulatory speed limits, the proposed models provide a better fit than the models by Bonneson et al. The improved fit is likely attributable to the different characteristics of two-lane highways with 75-mph regulatory speed limits. The state of Texas started posting 75-mph regulatory speed limits on selected rural highways relatively recently, and the higher speed limits are likely implemented only on highways that have gradual horizontal and vertical curvature, more generous cross-sectional design elements such as wider shoulders, and more sparsely populated area types that will have fewer driveways.

Four-Lane Highways

The functional form for the approach tangent speed model is shown in Equation 13. The results of the calibration for the right lane are shown in Table 16.

Table 16. Approach Tangent Speed Model Calibration Results for Four-Lane Highways – Right Lane

Model Statistics				
		R^2	0.63	
		RMSE, mph	5.6	
		Observations	29 sites (27,185 passenger cars)	
Range of Model Variables				
Variable	Variable Name	Units	Minimum	Maximum
$V_{t,85,pc}$	85 th Percentile Passenger Car Speed	mph	53.0	89.0
V_{sl}	Regulatory Speed Limit	mph	55	80
R	Radius of Curve	ft	865	5316
Calibrated Coefficient Values				
Coefficient	Coefficient Definition	Value	Std. dev	t-statistic
b_0	Intercept	9.46	0.16	60.2
b_1	Effect of Radius	-7.44	0.57	-13.1

The calibrated model is provided in Equation 19. A comparison of predicted and observed tangent speed values for the proposed model is provided graphically in Figure 9.

$$V_{t,85,pc} = 9.46\sqrt{V_{sl}}(1 - e^{-7.44(R+100)/5730}) \quad (18)$$

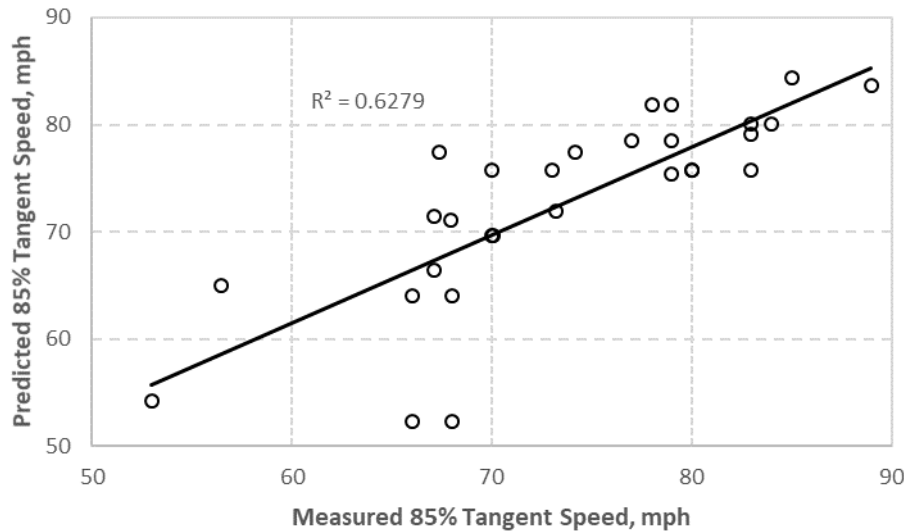


Figure 9. Comparison of Measured and Predicted Curve Speeds for Four-Lane Highways.

The functional form for the curve speed model was adopted from the analysis conducted by Bonneson et al. (2) and expanded to include variables to account for the travel lane (left or right lane) and the presence of undivided highway. It is described as follows:

$$v_c = \sqrt{\frac{15.0R_p(b_0 - b_1(1.47v_t) + 0.001b_2(1.47v_t)^2 + b_3I_{tk} + b_4I_{ln} + b_5I_U + \frac{e}{100})}{1 + 0.0322R_p b_2}} \leq v_t \quad (19)$$

where:

- I_{ln} = indicator variable for travel lane (= 1.0 if left lane, 0.0 if right lane); and
 I_U = indicator variable for undivided highway (= 1.0 if undivided, 0.0 if divided).

The results of the calibration are shown in Table 17. The values for coefficient b_4 show that drivers generally choose higher speeds in the left lane than in the right lane. The values for coefficient b_5 show that drivers choose lower speeds on curves on undivided highways when compared to curves on divided highways, perhaps out of desire to be cautious and avoid steering into the opposing lanes.

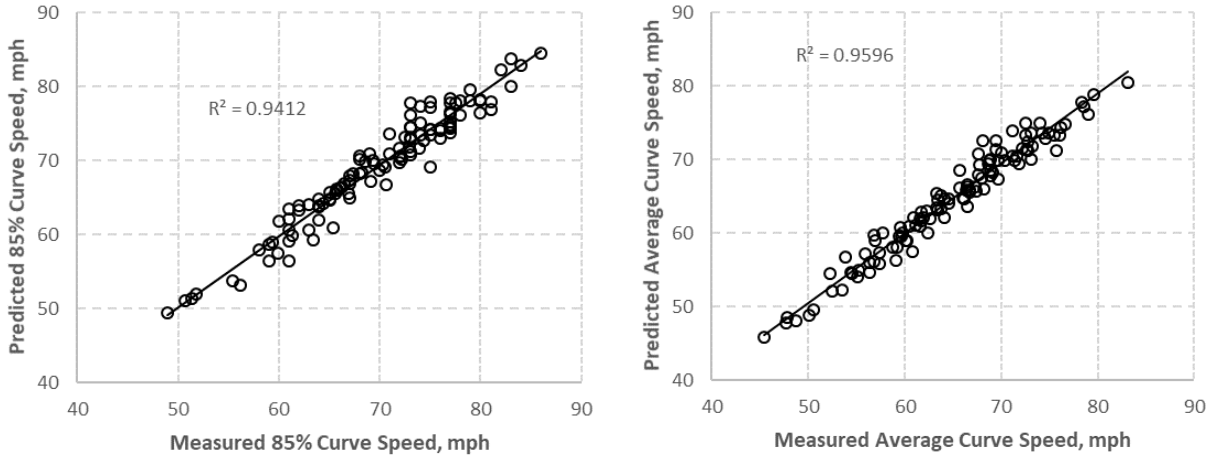
Table 17. Curve Speed Model Calibration Results for Four-Lane Highways.

Model Statistics		85 th Percentile Speed			Average Speed		
R^2		0.94			0.96		
RMSE, mph		1.9			1.6		
Observations		29 sites (27,185 passenger cars, 7838 trucks)					
Range of Model Variables							
Variable	Variable Name	Units	Min	Max	Units	Min	Max
V_t	Tangent speed	mph	51.4	90.0	mph	47.7	85.8
V_c	Curve speed	mph	49.0	86.0	mph	45.4	83.1
R	Radius of curve	ft	865	5316	ft	865	5316
I_c	Curve deflection angle	degrees	7	48	degrees	7	48
e	Superelevation rate	%	-0.065	0.11	%	-0.065	0.11
Calibrated Coefficient Values							
Coefficient	Coefficient Definition	Value	Std. dev	t-stat	Value	Std. dev	t-stat
b_0	Intercept	1.7152	0.5745	3.0	1.2826	0.3751	3.4
b_1	Effect of tangent speed	0.0181	0.0066	2.8	0.0148	0.0047	3.1
b_2	Effect of speed reduction	0.3129	0.1162	2.7	0.2872	0.0953	3.0
b_3	Effect of truck	-0.0510	0.0335	-1.5	-0.0342	0.0237	-1.4
b_4	Indicator for left lane	0.1027	0.0436	2.4	0.0880	0.0324	2.7
b_5	Indicator for undivided road	-0.2965	0.1197	-2.5	-0.2040	0.0752	-2.7

The calibrated models are provided in Equations 20 and 21. A comparison of predicted and observed tangent speed values for the proposed models is provided graphically in Figure 10, with each site represented by one data point for each combination of vehicle type (passenger car or truck) and lane (left or right).

$$v_{c,85} = \sqrt{\frac{15.0R_p(1.7152 + 0.0266v_{t,85} + 0.000676v_{t,85}^2 - 0.0510I_{tk} + 0.1027I_{ln} - 0.2965I_U + \frac{e}{100})}{1 + 0.0101R_p}} \leq v_{t,85} \quad (20)$$

$$v_{c,a} = \sqrt{\frac{15.0R_p \left(1.2826 + 0.0218v_{t,a} + 0.00621v_{t,a}^2 - 0.0342I_{tk} + 0.088I_{ln} - 0.204I_U + \frac{e}{100} \right)}{1 + 0.00925R_p}} \leq v_{t,a} \quad (21)$$



a. 85th-Percentile Speed

b. Average Speed

Figure 10. Comparison of Measured and Predicted Curve Speeds for Four-Lane Highways.

Other Empirical Relationships

In addition to the aforementioned speed prediction models, other linear models were calibrated to quantify the relationships between passenger car speeds and truck speeds, between 85th percentile speed and average speed, and between left-lane speeds and right-lane speeds on approach tangents. These analysis results are summarized in Table 18, Table 19, and Table 20. These coefficients can be used in combination with the tangent speed models (Equations 14, and 19) to obtain the needed average daytime truck speed for use with the curve speed models (Equations 17, and 22). The values for two-lane undivided highways with regulatory speed limits of ≤ 70 mph are provided for comparison purposes but are not used with the models described herein.

Table 18. Truck Speed as a Function of Passenger Car Speed at Approach Tangents.

Roadway Type	Calibration Coefficient (b_0)
2U ($V_{sl} \leq 70$ mph) (2)	0.97
2U ($V_{sl} = 75$ mph)	0.95
4U, 4D & 4F	0.95

Functional form: $V_{t,a,tk} = b_0 V_{t,a,pc}$.

$V_{t,a,tk}$ = average truck speed, $V_{t,a,pc}$ = average passenger car speed.

Table 19. Average Passenger Car Speed as a Function of 85th-Percentile Passenger Car Speed at Approach Tangents.

Roadway Type	Calibration Coefficient (b_0)
2U ($V_{sl} \leq 70$ mph) (2)	0.90
2U ($V_{sl} = 75$ mph)	0.92
4U, 4D & 4F	0.93

Functional form: $V_{t,a,pc} = b_0 V_{t,85,pc}$.

$V_{t,a,pc}$ = average passenger car speed, $V_{t,85,pc}$ = 85th percentile passenger car speed.

Table 20. Average Left-Lane Passenger Car Speed as a Function of Average Right-Lane Passenger Car Speed at Approach Tangents.

Roadway Type	Calibration Coefficient (b_0)
4U, 4D & 4F	1.04

Functional form: $V_{t,a,l-ln} = b_0 V_{t,a,r-ln}$.

$V_{t,a,l-ln}$ = average left-lane passenger car speed, $V_{t,a,r-ln}$ = average right-lane passenger car speed.

CHAPTER 4: SOFTWARE DEVELOPMENT AND ANALYSIS OF ELEVATION DATA

INTRODUCTION

This chapter describes efforts to update the software suite that is used to measure curve geometry and set curve advisory speeds. This software suite consists of the TRAMS executable program and the TCAS spreadsheet program that were developed in TxDOT Research Projects 0-5439 and 5-5439 (2, 3), as well as the Texas Curve Margin of Safety (TCMS) spreadsheet program that was developed in TxDOT Research Project 0-6714 (5) and updated in TxDOT Research Project 0-6932 (6).

The chapter is divided into two parts. The first part summarizes the software suite and describes efforts undertaken to update the programs. The second part provides a more detailed description of methods used to compute roadway grade, which is one of the additions to the software suite.

SOFTWARE PROGRAM DESCRIPTION AND UPDATES

The TRAMS and TCAS programs are used to implement TxDOT's GPS Method for conducting an engineering study to set curve advisory speeds. The GPS Method is conducted as follows:

1. Drive through a curve (or series of closely-spaced curves) with a test vehicle using a GPS receiver, an electronic ball-bank indicator, and a laptop computer running the TRAMS program.
2. Save the recorded and processed data log files from the test run.
3. Analyze the processed data using the TCAS spreadsheet to determine the curve advisory speed and (optionally) assess the need for other traffic control devices, such as Chevrons or delineators.

For single-curve applications, the TRAMS program relies on the user's ability to identify the starting and ending points of the curve, and it post-processes the raw GPS and ball-bank indicator data to identify the curve's sharpest arc and compute the radius and superelevation rate for that arc. Then, the TCAS spreadsheet uses these geometric inputs and an additional user-specified approach tangent speed or regulatory speed limit to compute the advisory speed. The TRAMS program archives both raw and processed data from the measurement devices.

Subsequent updates to the TCAS spreadsheet gave it the capability to process several closely-spaced curves using the archived raw data from a TRAMS test run (39). These updates were added to the TCAS spreadsheet and implemented in a macro-coding environment.

In this research project, the following updates were made to the TRAMS and TCAS programs:

- The TRAMS source code was moved to a new platform and recompiled to produce a software install package that is compatible with newer versions of Windows, particularly Windows 7 and 10. (The original TRAMS program was developed when Windows XP was the most common operating system.) Screenshots of the updated TRAMS program upon startup and while conducting a test run are shown in Figure 11 and Figure 12, respectively.
- Limitations on the time duration of a TRAMS run were removed so the user can conduct a continuous evaluation run of a highway section consisting of many curves.
- Data-logging functions for a barometer were added. The barometer is an optional device that can be used to measure elevation and compute roadway grade.
- The TCAS spreadsheet was incorporated into a larger spreadsheet program called the Texas Curve Evaluation Suite. TCES includes the following features:
 - A List worksheet, which consists of one row per curve. The List worksheet allows the user to import data describing a large number of curves from an extended TRAMS run to compute curve advisory speed for each curve.
 - A TCDs worksheet, which is identical to the Analysis worksheet within the previously developed TCAS spreadsheet.
 - A Pavement worksheet, which is identical to the Analysis worksheet within the previously developed TCMS spreadsheet.
- Data post-processing code was moved from TRAMS to its accompanying spreadsheet program. This change allows additional code changes to be made in the future without recompiling the TRAMS program.
- The data post-processing calculations for the electronic ball-bank indicator were improved to smooth extreme values. The improved ball-bank indicator reading is computed as the average of three consecutive readings instead of the raw reading from the device. The effect of this calculation is shown in Figure 13.

A screenshot of the List worksheet is shown in Figure 14. In addition to the data rows, the worksheet contains control buttons to allow the user to do the following:

- Process curve data from the most recently completed TRAMS test run.
- Process curve data from all TRAMS data files in the specified data folder.
- Compute results, including the rounded and unrounded advisory speeds, margin of safety, and skid number CMF for curves listed in the worksheet.
- Transfer data between the List and TCDs worksheets or the List and Pavement worksheets so the user can conduct a more detailed analysis of individual curves if needed.

Detailed instructions for installing and using the updated TRAMS and TCES programs are included in the *Horizontal Curve Evaluation Handbook* that was developed in parallel with this report.

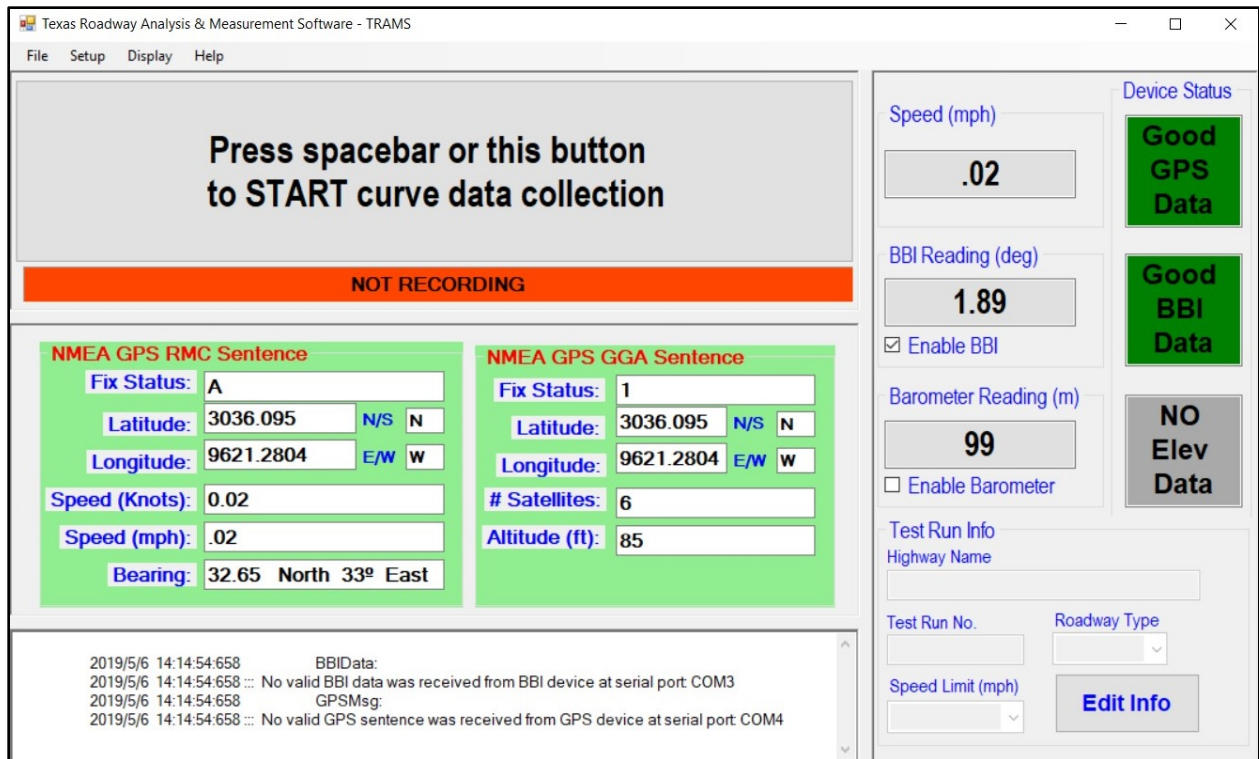


Figure 11. TRAMS upon Startup.

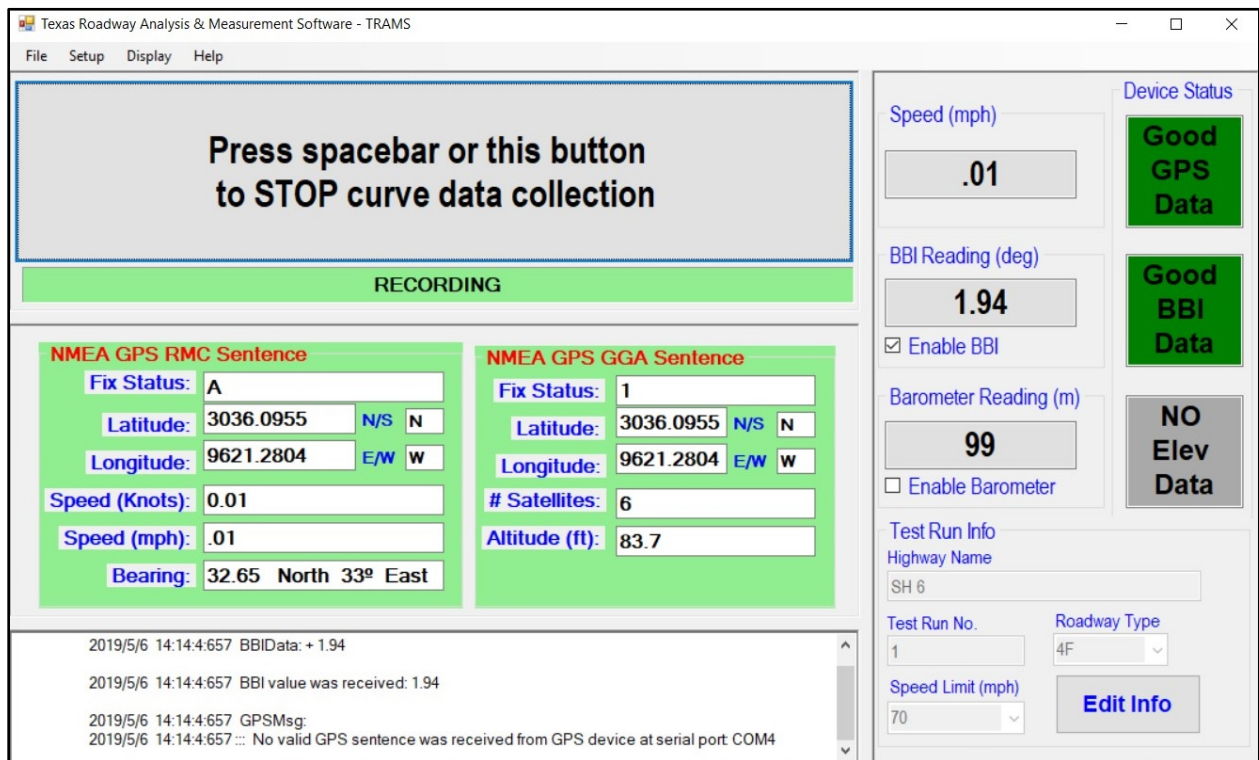


Figure 12. TRAMS in Use.

- Estimating speed differential between the midpoint and ending points of a curve.
- Computing side friction demand at specific points on a curve.

GPS provides elevation data and horizontal position data in two separate data sentences, which are designated as GGA and RMC, respectively (40). As a rule of thumb, it has been suggested that the error in GPS-measured elevation should be assumed as 50 percent greater than the error in GPS-measured horizontal position (41). Barometers (or barometric altimeters) provide measurements of elevation based on atmospheric pressure. For the purpose of computing roadway grade, elevation data need to be accurate in the relative sense (i.e., the change in elevation between subsequent points) but not in the absolute sense.

Preliminary Analysis

Figure 15 shows a comparison of elevation data measured from a device that contains a GPS receiver and a barometer. The GPS-measured elevation is shown in red and the barometer-measured elevation is shown in black. The two data series track each other, but with some error present in both.

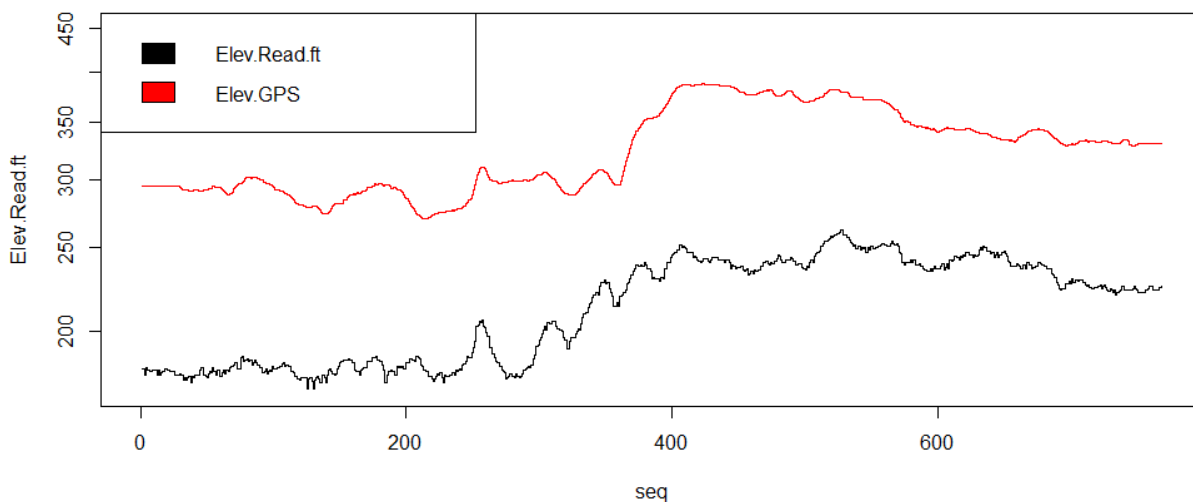


Figure 15. Comparison of Barometric and GPS Elevation.

Figure 16 shows an additional comparison of the data series with a vertical shift of 79.6 ft and a signal amplification of 14 percent on the barometer data series. As shown, the data series compare favorably when adjusted.

The researchers obtained ground-truth grade measurements collected from the field at 100-ft increments at three sites (Blue Ridge, Koppe Bridge, and Dogwood). The following process was used to compute the plotted grade measurements for the GPS and barometer devices:

1. Tabulate the elevation measurements that were recorded by the devices. These measurements were in increments of 20–30 ft, as influenced by test vehicle speed and device frequency.

2. Compute grade values between successive points as the difference in elevation divided by the distance traveled between points.
3. Interpolate the computed grade values to obtain grade estimates at the 100-ft increment points that correspond to the ground-truth grade data.

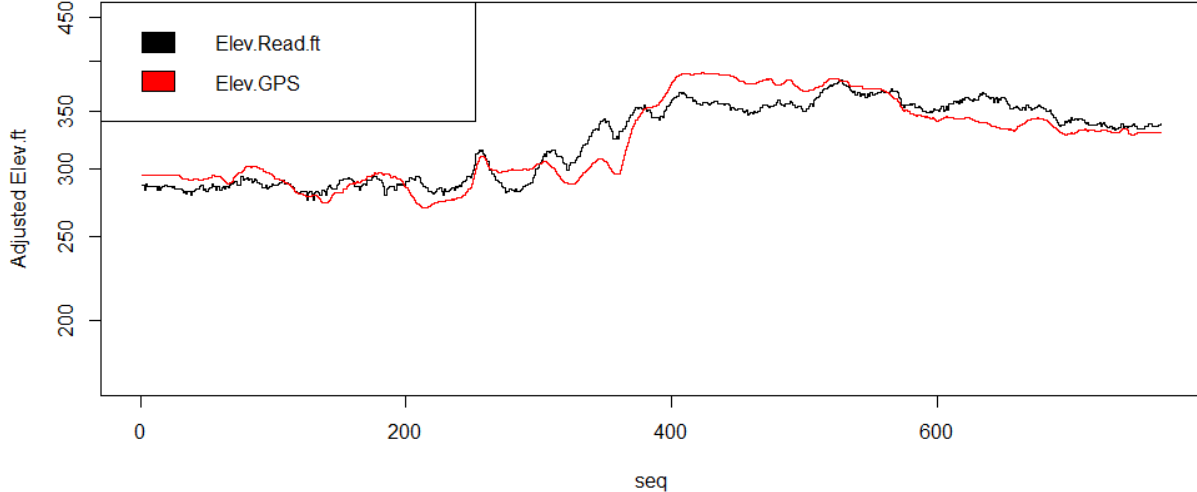


Figure 16. Adjusted Comparison of Barometric and GPS Elevation.

A comparison of GPS- and barometer-computed grade with ground-truth grade is shown in Figure 17. As shown, the grade values from both data streams generally track the ground-truth grade, but with some uncertainty and some unexpected spikes. The sources of these spikes could include vehicle bounce (which would cause vertical shifts) or device reporting latency (which would cause horizontal shifts). However, it appears that either data source could be adjusted to provide grade measurement of adequate accuracy for the purpose of conducting a curve margin-of-safety analysis.

Modeling Grade as a Function of Device Data

The researchers developed models of the road grade as a function of the data streams, GPS and barometer based, obtained from a device capable of producing both readings simultaneously. The ground-truth grade readings were then analyzed in conjunction with the device-based estimates (i.e., the three streams shown in Figure 17).

Modeling Framework

The researchers specified a mixed-effects model for the data streams allowing for time series characteristics. The general form is shown in Equation 22.

$$G_{ij} = (X_{ij} \cdot ML) \cdot \beta + \rho_i + \varepsilon_{ij} \quad (22)$$

where:

G_{ij} = grade at the i^{th} site at j^{th} reading point;

- X_{ij} = set of explanatory factors at i^{th} site and j^{th} reading, modeled as fixed underlying parameters;
 ML = matrix of lead/lag operators;
 β = coefficients correspondent to the explanatory factors;
 ρ_i = random intercept for i^{th} site; and
 ε_{ij} = error structure of the residual errors, potentially including codependency relationship within site i and reading j .

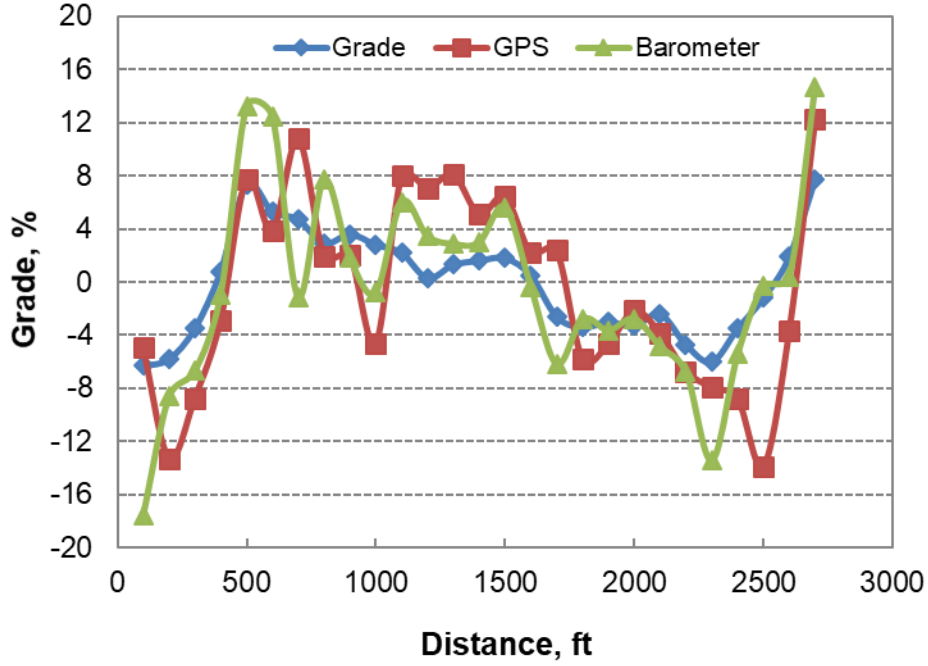


Figure 17. Comparison of Measured and Ground-Truth Grade.

The two main features of the model structure in Equation 22 are the application of a matrix of lag operators and the ability to incorporate codependency relationships in the error structure.

Matrix of Lead/Lag Operators

The matrix of lead/lag operators is partitioned into two subsets. Given that there are two explanatory variables (i.e., GPS and barometric grade estimates, respectively), the matrix is of dimension $2 \times (m+n)$ as follows:

$$ML = [ML_{GPS} | ML_{Barometer}] \quad (23)$$

The first partition corresponding to GPS readings is a matrix of dimensions $2m$ such that:

$$ML_{GPS} = \begin{bmatrix} L^0 & L^1 & \dots & L^{m-1} & L^m \\ 0 & 0 & \dots & 0 & 0 \end{bmatrix} \quad (24)$$

The second partition corresponding to barometer readings, is a matrix of dimensions $2n$:

$$ML_{Barometer} = \begin{bmatrix} 0 & 0 & \cdots & 0 & 0 \\ L^0 & L^1 & \cdots & L^{n-1} & L^n \end{bmatrix} \quad (25)$$

The lag operator is defined for a given time series as follows:

$$L \cdot X_t = X_{t-1} \quad (26)$$

A Lead operator is defined as follows:

$$Ld \cdot X_t = X_{t+1} \quad (27)$$

The researchers considered values of m and n in the above definitions up to five in the modeling process, for both lead and lag operators. As described later, an examination of the relationship between the ground truth values and the device estimates exhibited a lag in the devices (i.e., inflections of grade in the terrain appear to show up in the device streams at a slight delay, such as in Figure 18). For this reason, the final model described below included only lead operators and no lag operators.

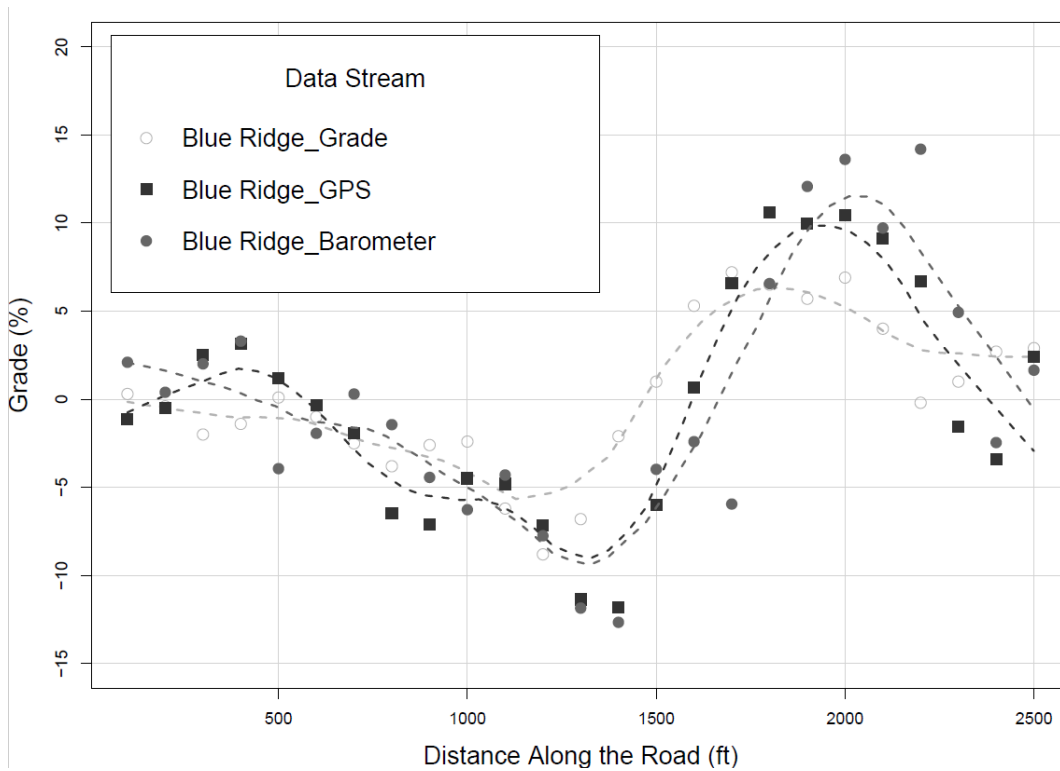


Figure 18. Comparison of Three Grade Measurement Time Series at Blue Ridge Site.

Codependency Error Structure

When handling a data stream collected as a time series (i.e., a sequence of data points close in time), it is very important to explicitly consider the likely codependence between observations as a function of their proximity in time. This need is more critical for situations of higher granularity in the time scale as is the case in the GPS and barometer data. The mixed-effects framework proposed by Pinheiro and Bates (42) is compatible with and allows the implementation of time series methods to account for error correlation structures. The general modeling structure accounts for three types of data features explicitly: (1) variables treated as fixed effects, which are expected to have “global” effects that are not time-dependent (e.g., a set of device readings and corresponding Lead/Lag operators); (2) variables treated as random effects, which can account for clusters or hierarchical structures in the data (such as in this case, different data streams collected at three different sites); and (3) specific types (i.e., structures) of time-dependency in the errors for a time series at any level of the dataset hierarchical structure.

For this particular analysis, the researchers implemented and tested the performance of an error structure at the lowest level of the hierarchical structure in the data. The methods implemented are those widely-accepted and used in modeling time series modeling originally proposed by Box et al. (43) and Tiao and Box (44).

The general model framework is known as Auto-Regressive Moving Average modeling (ARMA). This error specification accounts for the degree to which a given value in the time series is determined by prior values in the time series. Equation 28 shows the general form of the error structure under the ARMA specification.

$$\varepsilon_{ij} = \sum_{u=1}^p \delta_u \cdot L^u \varepsilon_{ij} + \sum_{v=1}^q \theta_v \cdot L^v \phi_{ij} + \phi_{ij} \quad (28)$$

where:

- ε_{ij} = residual at site i and reading j ;
- δ_u = coefficient for $L^u \varepsilon_{ij}$ in the combination of lagged residuals in ARMA model;
- θ_v = coefficient for $L^v \phi_{ij}$ in the combination of lagged residual nuances in ARMA model;
- $L^u \varepsilon_{ij}$ = lag u of residual (i.e., $L^u \varepsilon_{ij} = \varepsilon_{i,j-u}$);
- $L^v \phi_{ij}$ = lag v of residual nuance parameter (i.e., $L^v \phi_{ij} = \phi_{i,j-v}$);
- p = largest lag in the autoregressive part of the ARMA model; and
- q = largest lag in the moving average part of the ARMA model.

The error structure of the model is such that $\phi_{ij} \sim N[0, \sigma_0^2]$. The expected variance is estimated along with the rest of parameters in the model.

The researchers conducted regression analysis using open source statistical software and packages (42, 45, 46) to derive a smoothed model to estimate grade from GPS- or barometer-

based grade calculations. The analysis focused on ground-truth grade as the response variable and device-based grade calculations as predictor variables. A preliminary analysis without leads, lags or error correlation structure showed that GPS-measured grade values had an average error of 2.25 percent with no significant differences found between the three test sites. A model using both GPS-based grade values and barometer-based grade values had an average error of 2.06 percent. These models are described as follows:

$$G = 0.471G_{GPS} \quad (29)$$

$$G = 0.296G_{GPS} + 0.225G_{barom} \quad (30)$$

where:

- G = ground-truth grade, percent;
- G_{GPS} = GPS-based grade, percent; and
- G_{barom} = barometer-based grade, percent.

Both models show that a downscaling of the device-based values is needed to obtain an accurate measurement of grade. The model that uses both devices (Equation 30) does have a slightly lower error range than the model that uses only GPS (Equation 29), but the small difference does not justify requiring the use of a barometer.

A comparison of ground-truth, GPS-based, and barometer-based grade measurements suggested that device-based values have the tendency to lag, perhaps due to device latency or the response of the vehicle's suspension. This trend is illustrated in Figure 18. To improve the GPS-based estimate of grade, the researchers calibrated a model that includes two lead operators (to cancel away the lag in the series). As mentioned earlier, the research team tested up to five leads and lags but reduced the model by metrics of quality of information (i.e., Akaike Information Criterion). The most parsimonious model structure is described as follows:

$$G = b_0G_{GPS,0} + b_1G_{GPS,1} + b_2G_{GPS,2} \quad (31)$$

where:

- $G_{GPS,n}$ = n^{th} GPS-based grade estimate, percent.

After adding a co-dependency structure in the errors, the model calibration results are shown in Table 21, and the calibrated model is described in Equation 32. The error range for this model was found to be 1.63 percent, a notable improvement over the preliminary model described in Equation 29. Figure 19 shows the actual and estimated grades along the road for the Koppe Bridge site. Figure 20 shows how the estimated grade using Equation 32 compares to the actual grade at the three sites.

Table 21. Grade Time Series Model Calibration Results.

Model Coefficient	Definition	Value	Standard Error	t-stat	
b_0	Grade estimate at point 0	0.1991	0.0341	5.8	
b_1	Grade estimate at point 1 (following point 0)	0.1818	0.0317	5.7	
b_2	Grade estimate at point 2 (following points 0 and 1)	0.1943	0.0334	5.8	
Error Structure Coefficient	Definition	Value	χ^2 Statistic	Degrees of Freedom	p-value
δ_1	Lag-1 autocorrelation coefficient	0.9153	53.6715	2	<0.0001
δ_2	Lag-2 autocorrelation coefficient	-0.4115			

$$G = 0.1991G_{GPS,0} + 0.1818G_{GPS,1} + 0.1943G_{GPS,2} \quad (32)$$

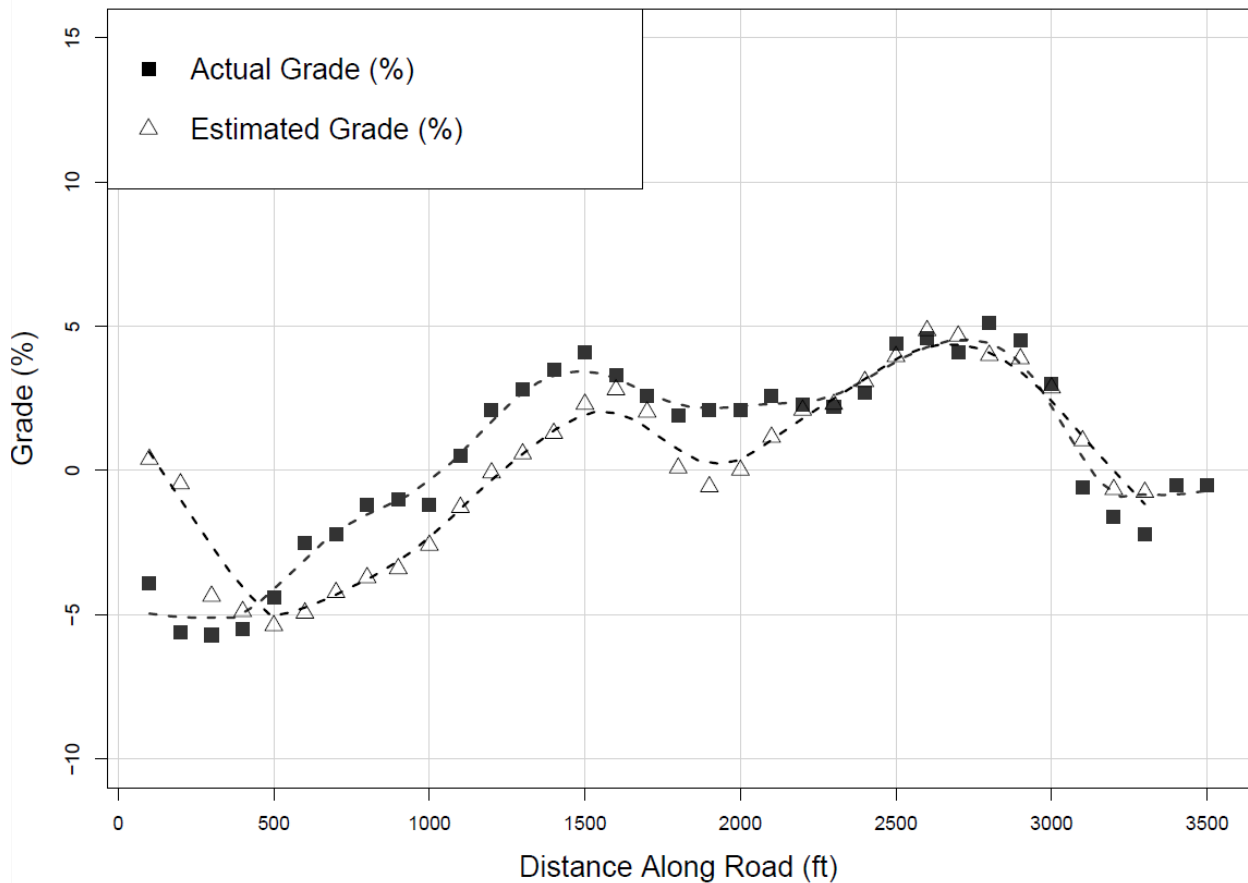


Figure 19. Performance of Grade-Calculation Model at Koppe Bridge Site.

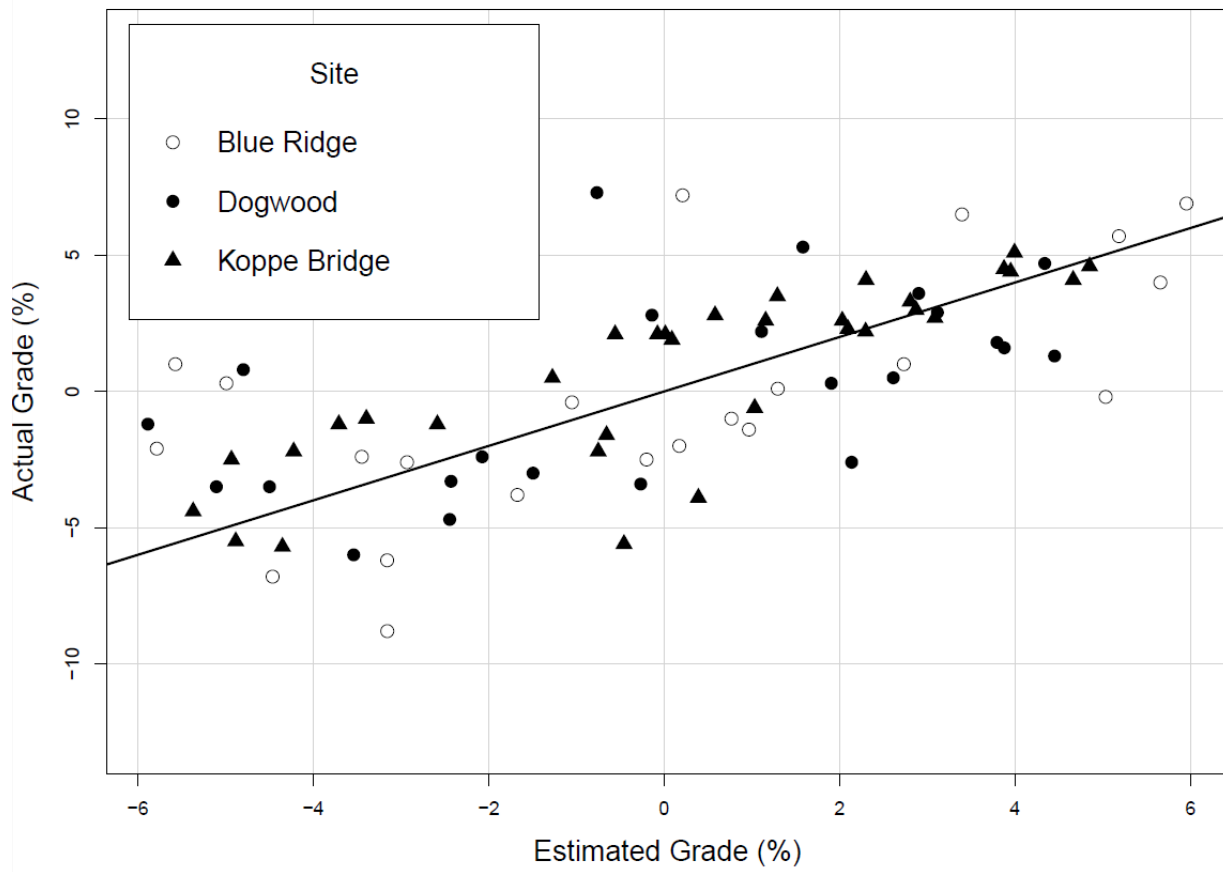


Figure 20. Comparison of Estimated and Actual Grade.

REFERENCES

- 1 *Texas MUTCD: Manual on Uniform Traffic Control Devices, Revision 1*. Texas Department of Transportation, Austin, Texas, 2012.
- 2 Bonneson, J., M. Pratt, J. Miles, and P. Carlson. *Development of Guidelines for Establishing Effective Curve Advisory Speeds*. Report FHWA/TX-07/0-5439-1, Texas Transportation Institute, College Station, Texas, 2007.
- 3 Bonneson, J., M. Pratt, J. Miles, and P. Carlson. *Procedures for Setting Advisory Speed: Course Notes—Appendix A. Horizontal Curve Signing Handbook, 2nd Edition*. Report FHWA/TX-09/5-5439-01-P1, Texas Transportation Institute, College Station, Texas, 2009.
- 4 *Procedures for Establishing Speed Zones*. Texas Department of Transportation, Austin, Texas, 2015.
- 5 Pratt, M., S. Geedipally, A. Pike, P. Carlson, A. Celozza, and D. Lord. *Evaluating the Need for Surface Treatments to Reduce Crash Frequency on Horizontal Curves*. Report FHWA/TX-14/0-6714-1, Texas A&M Transportation Institute, College Station, Texas, 2014.
- 6 Pratt, M., S. Geedipally, B. Wilson, S. Das, M. Brewer, and D. Lord. *Pavement Safety-Based Guidelines for Horizontal Curve Safety*. Report FHWA/TX-18/0-6932-R1, Texas A&M Transportation Institute, College Station, Texas, 2018.
- 7 Lord, D., M. Brewer, K. Fitzpatrick, S. Geedipally, and Y. Peng. *Analysis of Roadway Departure Crashes on Two-Lane Rural Roads in Texas*. Report FHWA/TX-11/0-6031-1, Texas Transportation Institute, College Station, Texas, 2011.
- 8 *A Policy on Geometric Design of Highways and Streets*. 5th Edition. American Association of State Highway and Transportation Officials, Washington, D.C., 2004.
- 9 McLean, J. Driver Speed Behaviour and Rural Road Alignment Design. In *Traffic Engineering and Control*, Vol. 22, No. 4, Transport Research Laboratory, Wokingham, Berkshire RG40 3GA United Kingdom, 1981, pp. 208–211.
- 10 Kanellaidis, G., J. Golias, and S. Efstathiadis. Drivers' speed behavior on rural road curves. In *Traffic Engineering and Control*, Vol. 31, No. 7/8, Laboratory of Highway Engineering, National Technical University of Athens, 1990, pp. 414–415.
- 11 Lamm, R., E. Choueiri, and T. Mailaender. Comparison of Operating Speeds on Dry and Wet Pavement of Two-Lane Rural Highways. In *Transportation Research Record: Journal of the Transportation Research Board*, No. 1280, TRB, National Research Council, Washington, D.C., 1990, pp. 199–207.
- 12 Cruzado, I., D. Valdes, and C. Calero. Speed and Design Consistency of Combined Horizontal and Vertical Alignments in Two-Lane Rural Roads. University Transportation Research Center—Region 2, Contract 49997-39-24, 2014.
- 13 Ottesen, J., and R. Krammes. Speed Profile Model for a Design Consistency Evaluation Procedure in the United States. In *Transportation Research Record: Journal of the Transportation Research Board*, No. 1701, TRB, National Research Council, Washington, D.C., 2000, pp. 76–85.
- 14 Collins, K., and R. Krammes. Preliminary Validation of a Speed-Profile Model for Design Consistency Evaluation. In *Transportation Research Record*, No. 1523, TRB, National Research Council, Washington, D.C., 1996, pp. 11–21.
- 15 Misaghi, P., and Y. Hassan. Modeling Operating Speed and Speed Differential on Two-Lane Rural Roads. *Journal of Transportation Engineering*, Vol. 131, No. 6, 2005, pp. 408–417.

- 16 Schurr, S., P. McCoy, G. Pesti, and R. Huff. Relationship of Design, Operating, and Posted Speeds on Horizontal Curves of Rural Two-Lane Highways in Nebraska. In *Transportation Research Record: Journal of the Transportation Research Board*, No. 1796, TRB, Washington, D.C., 2002, pp. 60–71.
- 17 Gong, H., and N. Stamatiadis. Operating Speed Prediction Models for Horizontal Curves on Rural Four-Lane Highways. In *Transportation Research Record: Journal of the Transportation Research Board*, No. 2075, TRB, National Research Council, Washington, D.C., 2008, pp. 1–7.
- 18 Cheng, Y., F. Chen, X. Huang, F. Wang, and M. Liu. “Predicting Operating Speed on Curve Sections of Eight-Lane Expressway in Plain Area.” Presented at the 4th International Symposium on Highway Geometric Design.
- 19 Montella, A., L. Pariota, F. Galante, L. Imbriana, and F. Mauriello. Prediction of Drivers’ Speed Behavior on Rural Motorways Based on an Instrumented Vehicle Study. In *Transportation Research Record: Journal of the Transportation Research Board*, No. 2434, TRB, National Research Council, Washington, D.C., 2014, pp. 52–62.
- 20 Semeida, A. Application of artificial neural networks for operating speed prediction at horizontal curves: a case study in Egypt. In *Journal of Modern Transportation*, Vol. 22, No. 1, 2014, pp. 20–29.
- 21 Morris, C., E. Donnell. Passenger Car and Truck Operating Speed Models on Multilane Highways with Combinations of Horizontal Curves and Steep Grades. In *American Society of Civil Engineers: Journal of the Transportation Engineering*, Vol. 140, No. 11, 2014, pp. 1–10.
- 22 Fitzpatrick, K., L. Elefteriadou, D. Harwood, J. Collins, J. McFadden, I. Anderson, R. Krammes, N. Irizarry, K. Parma, K. Bauer, and K. Passetti. *Speed Prediction for Two-Lane Rural Highways*. FHWA-RD-99-171. Federal Highway Administration, U.S. Department of Transportation, Washington, D.C., 2000.
- 23 Bonneson, J., and M. Pratt. *Roadway Safety Design Workbook*. Report FHWA/TX-09-0-4703-P2, Texas Transportation Institute, College Station, Texas, 2009.
- 24 Lalani, N. 1991. “Comprehensive Safety Program Produces Dramatic Results.” In *ITE Journal*, Vol. 61, No. 10, Institute of Transportation Engineers, 1991, pp. 31–34.
- 25 Srinivasan, R., J. Baek, D. Carter, B. Persaud, C. Lyon, K. A. Eccles, F. Gross, and N. X. Lefler. *Safety Evaluation of Improved Curve Delineation*. Report FHWA-HRT-09-045, VHB, Vienna, Virginia, 2009.
- 26 Choi, Y.-Y., S.-Y. Kho, C. Lee, and D.-K. Kim. “Development of Crash Modification Factors of Alignment Elements and Safety Countermeasures for Korean Freeways.” Paper No. 15-0503. Presented at the 94th Annual Meeting of the Transportation Research Board, Washington, D.C., 2015.
- 27 Montella, A. Safety Evaluation of Curve Delineation Improvements Empirical Bayes Observational Before-and-After Study. In *Transportation Research Record: Journal of the Transportation Research Board*, No. 2103, TRB, National Research Council, Washington, D.C., 2009, pp. 69–79.
- 28 Tsyganov, A. R., R. B. Machemehl, and N. Warrenchuk. “Driver Performance and Safety Effects of Edge Lines on Rural Two-Lane Highways.” Paper No. 09-0751. Presented at the 88th Annual Meeting of the Transportation Research Board, Washington, D.C., 2009.
- 29 Elvik, R., and T. Vaa. *The Handbook of Road Safety Measures*. Oxford, United Kingdom: Elsevier, 2004.

- 30 Gillespie, T.D. *Fundamentals of Vehicle Dynamics*. Society of Automotive Engineers: Warrendale, Pennsylvania, 1992.
- 31 Alessandroni, G., A. Carini, E. Lattanzi, V. Freschi, and A. Bogliolo. A Study on the Influence of Speed on Road Roughness Sensing: The SmartRoadSense Case. In *Sensors*, Vol. 17, No. 2, 2017.
- 32 Iwase, T., K. Nakasaki, Y. Namikawa, and T. Mori. On sound spectral model of road vehicle for prediction of road traffic noise: Considerations for establishing the ASJ RTN-Model 2003. In *Acoustic Science and Technology*, Vol. 26, No. 1, 2005.
- 33 Karamihas, S., T. Gillespie, R. Perera, and S. Kohn. *Guidelines for Longitudinal Pavement Profile Measurement*. NCHRP Report 434, Transportation Research Board, Washington, D.C., 1999.
- 34 Van Ruth, F. Traffic intensity as indicator of regional economic activity, Discussion paper 2014/21, Statistics Netherlands, 2014.
- 35 Liu, X., Z. Zhang, G. Li, and T. Lv. Research on technology of traffic video incidents detection under highway condition. In *The Journal of China Universities of Posts and Telecommunications*, Vol. 17, No. 1, 2010, pp. 79–83.
- 36 Tsai, Y., and C. Ai. “An Automated Superelevation Measurement Method for Horizontal Curve Safety Assessment Using a Low-Cost Mobile Device.” Paper No. 17-04607. Presented at the 96th Annual Meeting of the Transportation Research Board, Washington, D.C., 2017.
- 37 Cleveland, W., E. Grosse, and W. Shyu. Local Regression Models. In *Statistical Models in S*, Wadsworth and Brooks, Pacific Grove, California, 1992, pp. 309–376.
- 38 *SAS/STAT User’s Guide, Version 9.2*. Second Edition, SAS Institute, Inc., Cary, North Carolina, 2009.
- 39 Carlson, P., M. Pratt, L. Higgins, and A. Nelson. *Traffic Control Device Evaluation Program: Technical Report*. Report FHWA/TX-14/9-1001-4, College Station, Texas, 2014.
- 40 NMEA Data. <http://www.gpsinformation.org/dale/nmea.htm>. Accessed July 21, 2017.
- 41 Altitude Accuracy. <http://gpsinformation.net/main/altitude.htm>. Accessed July 21, 2017.
- 42 Pinheiro, J., and D. Bates. *Mixed-Effects Models in S and S-PLUS*. Springer, New York, New York, 2000.
- 43 Box, G., G. Jenkins, G. Reinsel, and G. Ljung. *Time Series Analysis: Forecasting and Control, Fifth Edition*. John Wiley and Sons, 2015.
- 44 Tiao, G., and G. Box. Modeling Multiple Time Series with Applications. In *Journal of American Statistical Association*, Vol. 76, No. 376, 1981, pp. 802-816.
- 45 R: A Language and Environment for Statistical Computing. <http://www.R-project.org>. Accessed April 30, 2013.
- 46 Bates, D., M. Mächler, B. Bolker, and S. Walker. Fitting Linear Mixed-Effects Models using lme4. In *Journal of Statistical Software*, Vol. 67, No. 1, 2015, pp. 1-48.

